NUCL SCI TECH (2018) 29:82
https://doi.org/10.1007/s41365-018-0425-x

Kinetic freeze-out temperatures in central and peripheral collisions: which one is larger?

Hai-Ling Lao[1] · Fu-Hu Liu[1] · Bao-Chun Li[1] · Mai-Ying Duan[1]

Received: 15 January 2018 / Revised: 10 February 2018 / Accepted: 18 February 2018 / Published online: 26 April 2018

Abstract The kinetic freeze-out temperatures, T_0, in nucleus–nucleus collisions at the Relativistic Heavy Ion Collider (RHIC) and Large Hadron Collider (LHC) energies are extracted by four methods: (1) the Blast-Wave model with Boltzmann–Gibbs statistics (the BGBW model), (2) the Blast-Wave model with Tsallis statistics (the TBW model), (3) the Tsallis distribution with flow effect (the improved Tsallis distribution), and (4) the intercept in $T = T_0 + am_0$ (the alternative method), where m_0 denotes the rest mass and T denotes the effective temperature which can be obtained by different distribution functions. It is found that the relative sizes of T_0 in central and peripheral collisions obtained by the conventional BGBW model which uses a zero or nearly zero transverse flow velocity, β_T, are contradictory in tendency with other methods. With a re-examination for β_T in the first method, in which β_T is taken to be $\sim(0.40 \pm 0.07)c$, a recalculation presents a consistent result with others. Finally, our results show that the kinetic freeze-out temperature in central collisions is larger than that in peripheral collisions.

Keywords Kinetic freeze-out temperature · Methods for extraction · Central collisions · Peripheral collisions

This work was supported by the National Natural Science Foundation of China (Nos. 11575103 and 11747319), the Shanxi Provincial Natural Science Foundation (No. 201701D121005), and the Fund for Shanxi "1331 Project" Key Subjects Construction.

✉ Fu-Hu Liu
fuhuliu@163.com; fuhuliu@sxu.edu.cn

[1] Institute of Theoretical Physics and State Key Laboratory of Quantum Optics and Quantum Optics Devices, Shanxi University, Taiyuan 030006, China

1 Introduction

Temperature is an important concept in high-energy nucleus–nucleus collisions. Usually, three types of temperatures which contain the chemical freeze-out temperature, kinetic freeze-out temperature, and effective temperature are used in the literature [1–5]. The chemical freeze-out temperature describes the excitation degree of the interacting system at the stage of chemical equilibrium in which the chemical components (relative fractions) of particles are fixed. The kinetic freeze-out temperature describes the excitation degree of the interacting system at the stage of kinetic and thermal equilibrium in which the (transverse) momentum spectra of particles are no longer changed. The effective temperature is not a real temperature. In fact, the effective temperature is related to particle mass and can be extracted from the transverse momentum spectra by using some distribution laws such as the standard (Boltzmann, Fermi–Dirac, and Bose–Einstein), Tsallis, and so forth.

Generally, the chemical freeze-out temperature is usually obtained from the particle ratios [6–8]. It is equal to or larger than the kinetic freeze-out temperature due to the chemical equilibrium during or earlier than the kinetic equilibrium. The effective temperature is larger than the kinetic freeze-out temperature due to mass and flow effects [9, 10]. Both the chemical freeze-out and effective temperatures in central nucleus–nucleus collisions are larger than those in peripheral collisions due to more violent interactions occurring in central collisions. In fact, central collisions contain more nucleons, and peripheral collisions contain less nucleons. Usually, there are small dissents in the extractions of chemical freeze-out temperature and effective temperature. As for the extraction of kinetic freeze-out temperature, the situations are largely non-uniform.

Currently, four main methods are used in the extraction of kinetic freeze-out temperature, T_0, which are (1) the Blast-Wave model with Boltzmann–Gibbs statistics (the BGBW model) [11–13], (2) the Blast-Wave model with Tsallis statistics (the TBW model) [14], (3) the Tsallis distribution with flow effect (the improved Tsallis distribution) [15, 16], and (4) the intercept in $T = T_0 + am_0$ (the alternative method) [12, 17–20], where m_0 denotes the rest mass and T denotes the effective temperature which can be obtained by different distribution functions. In detail, the alternative method can be divided into a few sub-methods due to different distributions being used. Generally, we are inclined to use the standard and Tsallis distributions in the alternative method due to the standard distribution being closest to the ideal gas model in thermodynamics, and the Tsallis distribution describing a wide spectrum which needs a two- or three-component standard distribution to be fitted [21].

The kinetic freeze-out temperature, T_0, and the mean transverse radial flow velocity, β_T, can be simultaneously extracted by the first three methods. The alternative method needs further treatments in extracting the flow velocity. In our recent works [22–24], the mean transverse flow velocity, β_T, is regarded as the slope in the relation $\langle p_T \rangle = \langle p_T \rangle_0 + \beta_T \overline{m}$, where $\langle p_T \rangle$ denotes the mean value of transverse momenta p_T, $\langle p_T \rangle_0$ denotes the mean transverse momentum in the case of zero flow velocity, and $\overline{m}$ denotes the mean moving mass. The mean flow velocity, β, is regarded as the slope in the relation $\langle p \rangle = \langle p \rangle_0 + \beta \overline{m}$, where $\langle p \rangle$ denotes the mean value of momenta, p, and $\langle p \rangle_0$ denotes the mean momentum in the case of zero flow velocity. Although the mean transverse radial flow and mean transverse flow are not exactly the same, we use the same symbol to denote their velocities and neglect the difference between them. In fact, the mean transverse radial flow contains only the isotropic flow, and the mean transverse flow contains both the isotropic and anisotropic flows. The isotropic flow is mainly caused by isotropic expansion of the interacting system, and the anisotropic flow is mainly caused by anisotropic squeeze between two incoming nuclei.

We are interested in the coincidence and difference among the four methods in the extractions of T_0 and β_T. In this paper, we shall use the four methods to extract T_0 and β_T from the p_T spectra of identified particles produced in central and peripheral gold–gold (Au–Au) collisions at the center-of-mass energy per nucleon pair $\sqrt{s_{NN}} = 200$ GeV (the top RHIC energy) and in central and peripheral lead–lead (Pb–Pb) collisions at $\sqrt{s_{NN}} = 2.76$ TeV (one of the LHC energies). The model results on the p_T spectra are compared with the experimental data of the PHENIX [25], STAR [26, 27], and ALICE Collaborations [28, 29], and the model results on T_0 and β_T in different collisions and by different methods are compared each other.

The rest of this paper is structured as follows. The formalism and method are shortly described in Sect. 2. Results and discussion are given in Sect. 3. Finally, we summarize our main observations and conclusions in Sect. 4.

2 Formalism and method

The four methods can be found in related references [11–20]. To give a whole representation of this paper, we present directly and concisely the four methods in the following. In the representation, some quantities such as the kinetic freeze-out temperature, the mean transverse (radial) flow velocity, and the effective temperature in different methods are uniformly denoted by T_0, β_T and T, respectively, though different methods correspond to different values. All of the model descriptions are presented at the mid-rapidity which uses the rapidity $y \approx 0$ and results in $\cosh(y) \approx 1$ which appears in some methods. At the same time, the spin property and chemical potential in the p_T spectra are neglected due to their small influences in high-energy collisions. This means that we can give up the Fermi–Dirac and Bose–Einstein distributions and use only the Boltzmann distribution in the case of considering the standard distribution.

According to Refs. [11–13], the BGBW model results in the p_T distribution to be

$$f_1(p_T) = C_1 p_T m_T \int_0^R r\mathrm{d}r \times I_0\left[\frac{p_T \sinh(\rho)}{T_0}\right] K_1\left[\frac{m_T \cosh(\rho)}{T_0}\right], \tag{1}$$

where C_1 is the normalized constant which results in $\int_0^\infty f_1(p_T)\mathrm{d}p_T = 1$, where I_0 and K_1 are the modified Bessel functions of the first and second kinds, respectively, $m_T = \sqrt{p_T^2 + m_0^2}$ is the transverse mass, $\rho = \tanh^{-1}[\beta(r)]$ is the boost angle, $\beta(r) = \beta_S (r/R)^{n_0}$ is a self-similar flow profile, β_S is the flow velocity on the surface of the thermal source, r / R is the relative radial position in the thermal source, and n_0 is a free parameter which is customarily chosen to be 2 [11] due to this quadratic profile resembling the solutions of hydrodynamics closest [30]. Generally, $\beta_T = (2/R^2) \int_0^R r\beta(r)\mathrm{d}r = 2\beta_S/(n_0 + 2)$. In the case of $n_0 = 2$, as used in Ref. [11], we have $\beta_T = 0.5\beta_S$ [31].

According to Ref. [14], the TBW model results in the p_T distribution to be

$$f_2(p_T) = C_2 p_T m_T \int_{-\pi}^{\pi} d\phi \int_0^R r dr \{1 + \frac{q-1}{T_0}[m_T \cosh(\rho) - p_T \sinh(\rho)\cos(\phi)]\}^{-q/(q-1)}, \quad (2)$$

where C_2 is the normalized constant which results in $\int_0^\infty f_2(p_T)dp_T = 1$, q is an entropy index characterizing the degree of non-equilibrium, and ϕ denotes the azimuth. In the case of $n_0 = 1$, as used in Ref. [14], we have $\beta_T = 2\beta_S/(n_0+2) = (2/3)\beta_S$ due to the same flow profile as in the BGBW model. We would like to point out that the index $-q/(q-1)$ in Eq. (2) replaced $-1/(q-1)$ in Ref. [14] due to q being very close to 1. In fact, the difference between the results corresponding to $-q/(q-1)$ and $-1/(q-1)$ are small in the Tsallis distribution [32].

According to Refs. [15, 16], the improved Tsallis distribution in terms of p_T is

$$\begin{aligned} f_3(p_T) = C_3\{&2T_0[rI_0(s)K_1(r) - sI_1(s)K_0(r)] \\ &- (q-1)T_0r^2I_0(s)[K_0(r)+K_2(r)] \\ &+ 4(q-1)T_0rsI_1(s)K_1(r) \\ &- (q-1)T_0s^2K_0(r)[I_0(s)+I_2(s)] \\ &+ \frac{(q-1)}{4}T_0r^3I_0(s)[K_3(r)+3K_1(r)] \\ &- \frac{3(q-1)}{2}T_0r^2s[K_2(r)+K_0(r)]I_1(s) \\ &+ \frac{3(q-1)}{2}T_0s^2r[I_0(s)+I_2(s)]K_1(r) \\ &- \frac{(q-1)}{4}T_0s^3[I_3(s)+3I_1(s)]K_0(r)\}, \end{aligned} \quad (3)$$

where C_3 is the normalized constant which results in $\int_0^\infty f_3(p_T)dp_T = 1$, $r \equiv \gamma m_T/T_0$, $s \equiv \gamma\beta_T p_T/T_0$, $\gamma = 1/\sqrt{1-\beta_T^2}$, and $I_{0-3}(s)$ and $K_{0-3}(r)$ are the modified Bessel functions of the first and second kinds, respectively.

As for the alternative method [12, 17–20, 22–24], to use the relations $T = T_0 + am_0$, $\langle p_T\rangle = \langle p_T\rangle_0 + \beta_T\overline{m}$, and $\langle p\rangle = \langle p\rangle_0 + \beta\overline{m}$, we can choose the standard and Tsallis distributions to fit the p_T spectra of identified particles produced in high-energy collisions. Because we give up the Fermi–Dirac and Bose–Einstein distributions, only the Boltzmann distribution is used in the case of considering the standard distribution in the present work. Both the Boltzmann and Tsallis distributions have more than one forms. We choose the form of Boltzmann distribution [33]

$$f_{4a}(p_T) = C_{4a} p_T m_T \exp\left(-\frac{m_T}{T}\right) \quad (4)$$

and the form of Tsallis distribution [32, 33]

$$f_{4b}(p_T) = C_{4b} p_T m_T \left(1 + \frac{q-1}{T}m_T\right)^{-q/(q-1)}, \quad (5)$$

where C_{4a} and C_{4b} are the normalized constants which result in $\int_0^\infty f_{4a}(p_T)dp_T = 1$ and $\int_0^\infty f_{4b}(p_T)dp_T = 1$ respectively.

It should be noticed that the above five distributions are only valid for the spectra in a low-p_T range. That is, they describe only the soft excitation process. Even if for the soft process, the Boltzmann distribution is not always enough to fit the p_T spectra in some cases. In fact, two- or three-component Boltzmann distributions can be used if necessary, in which T is the average weight at the effective temperatures obtained from different components. We have

$$f_{4a}(p_T) = \sum_{i=1}^{l} k_i C_{4ai} p_T m_T \exp\left(-\frac{m_T}{T_i}\right) \quad (6)$$

and

$$T = \sum_{i=1}^{l} k_i T_i, \quad (7)$$

where $l = 2$ or 3 denotes the number of components, and k_i, C_{4ai}, and T_i denote the contribution ratio (relative contribution or fraction), normalization constant, and effective temperature related to the i-th component, respectively. As can be seen in the next section, Eqs. (6) and (7) are not needed in the present work because only simple component Boltzmann distribution, i.e. Eq. (4), is used in the analyses. We present here Eqs. (6) and (7) to point out a possible application in future.

For the spectra in a wide p_T range which contains low and high p_T regions, we have to consider the contribution of a hard scattering process. Generally, the contribution of a hard process is parameterized to an inverse power-law

$$f_H(p_T) = Ap_T\left(1 + \frac{p_T}{p_0}\right)^{-n} \quad (8)$$

which is resulted from the QCD (quantum chromodynamics) calculation [34–36], where p_0 and n are free parameters, and A is the normalized constant which depends on p_0 and n and results in $\int_0^\infty f_H(p_T)dp_T = 1$.

To describe the spectra in a wide p_T range, we can use a superposition of both contributions of soft and hard processes. The contribution of the soft process is described by one of the BGBW models, the TBW model, the improved Tsallis distribution, the Boltzmann distribution or two- or three-component Boltzmann distributions, and the Tsallis distribution, while the contribution of hard process is described by the inverse power-law. We have the superposition

$$f_0(p_T) = kf_S(p_T) + (1-k)f_H(p_T), \quad (9)$$

where k denotes the contribution ratio of the soft process and results naturally in $\int_0^\infty f_0(p_T)dp_T = 1$, and $f_S(p_T)$ denotes one of the five distributions discussed in the four methods.

It should be noted that Eq. (9) and its components $f_S(p_T)$ and $f_H(p_T)$ are probability density functions. The experimental quantity of p_T distribution has mainly three forms, dN/dp_T, $d^2N/(dydp_T)$, and $(2\pi p_T)^{-1}d^2N/(dydp_T)$, where N denotes the number of particles and dy is approximately treated as a constant due to it being usually a given and small value at the mid-rapidity. To connect Eq. (9) with dN/dp_T, we need a normalization constant, N_0. To connect Eq. (9) with $d^2N/(dydp_T)$, we need another normalization constant, N_0. To connect Eq. (9) with $(2\pi p_T)^{-1}d^2N/(dydp_T)$, we have to rewrite Eq. (9) to $f_0(p_T)/p_T = [kf_S(p_T) + (1-k)f_H(p_T)]/p_T$ and compare the right side of the new equation with the data with a new normalization constant, N_0.

3 Results and discussion

Figure 1 presents the transverse momentum spectra, $(2\pi p_T)^{-1}d^2N/(dydp_T)$, of (a)–(c) positively charged pions (π^+), positively charged kaons (K^+), neutral kaons (K_S^0 only), and protons (p), as well as (b)–(d) negatively charged pions (π^-), negatively charged kaons (K^-), neutral kaons (K_S^0 only), and antiprotons ($\bar{p}$) produced in (a)–(b) central (0–5 and 0–12%) and (c)–(d) peripheral (80–92 and 60–80%) Au–Au collisions at $\sqrt{s_{NN}} = 200$ GeV, where the spectra for different types of particles and for the same or similar particles in different conditions are multiplied by different amounts shown in the panels for clarity and normalization. The closed symbols represent the experimental data of the PHENIX Collaboration measured in the pseudorapidity range $|\eta| < 0.35$ [25]. The open symbols represent the STAR data measured in the rapidity range $|y| < 0.5$ [26, 27], where the data for K^+ and K^- are not available and the data for K_S^0 in (a)–(c) and (b)–(d) are the same. The solid, dashed, dotted, dashed-dotted, and dashed-dotted-dotted curves are our results calculated by using the superpositions of (1) the BGBW model (Eq. 1) and inverse power-law (Eq. 8), (2) the TBW model (Eq. 2) and inverse power-law, (3) the improved Tsallis distribution (Eq. 3) and inverse power-law, $(4)_a$ the Boltzmann distribution (Eq. 4) and inverse power-law, as well as $(4)_b$ the Tsallis distribution (Eq. 5) and inverse power-law, respectively. These different superpositions are also different methods for fitting the data. The values of free parameters T_0, β_T, k, p_0, and n, normalization constant, N_0, which is used to fit the data by a more accurate method comparing with Ref. [37], and χ^2 per degree of freedom (χ^2/dof) corresponding to the fit of method (1) are listed in Table 1; the values of T_0, q, β_T, k, p_0, n, N_0, and χ^2/dof corresponding to methods (2) and (3) are listed in Tables 2 and 3 respectively; the values of T, k, p_0, n, N_0, and χ^2/dof corresponding to methods $(4)_a$ are listed in Table 4; and the values of T, q, k, p_0, n, N_0, and χ^2/dof corresponding to method $(4)_b$ are listed in Table 5. One can see that, in most cases, all of the considered methods describe approximately the p_T spectra of identified particles produced in central and peripheral Au–Au collisions at $\sqrt{s_{NN}} = 200$ GeV.

Figure 2 is the same as Fig. 1, but it shows the spectra, $(1/N_{EV})(2\pi p_T)^{-1}d^2N/(dydp_T)$, (a)–(c) π^+ $(\pi^+ + \pi^-)$, K^+ $(K^+ + K^-)$, and p $(p + \bar{p})$, as well as (b)–(d) π^- $(\pi^+ + \pi^-)$, K^- $(K^+ + K^-)$, and $\bar{p}$ $(p + \bar{p})$ produced in (a)–(b) central (0–5%) and (c)–(d) peripheral (80–90 and 60–80%) Pb–Pb collisions at $\sqrt{s_{NN}} = 2.76$ TeV, where N_{EV} is on the vertical axis and denotes the number of events, which is usually omitted. The closed (open) symbols represent the experimental data of the ALICE Collaboration measured in $|y| < 0.5$ [28] (in $|\eta| < 0.8$ for the high p_T region and in $|y| < 0.5$ for the low p_T region [29]). The data for $\pi^+ + \pi^-$, $K^+ + K^-$, and $p + \bar{p}$ in (a)–(c) and (b)–(d) are the same. One can see that, in most cases, all of the considered methods describe approximately the p_T spectra of identified particles produced in central and peripheral Pb–Pb collisions at $\sqrt{s_{NN}} = 2.76$ TeV. Because the values of χ^2/dof in most cases are greater than 2 and sometimes as large as 20.5, the fits in Figs. 1 and 2 are only approximate and qualitative. The large values of χ^2/dof in the present work are caused by two factors which are the very small errors in the data and large dispersion between the curve and data in some cases. It is hard to reduce the values of χ^2/dof in our fits.

In the above fits, we have an addition term of inverse power-law to account for hard process. This part contributes a small fraction to the p_T spectra, though the contribution coverage is wide. In the fitting procedure, according to the changing tendency of data in a low p_T range from 0 to 2 GeV/c, the part for the soft process can be well constrained first of all, though the contribution of the soft process can even reach 3.5 GeV/c. Then, the part for the hard process can be also constrained conveniently. In addition, in order to get a set of fitted parameters as accurately as possible, we use the least square method in the whole p_T coverage. It seems that different fitted parameters can be obtained in different p_T coverages. We should use a p_T coverage as widely as possible, especially for the extraction of the parameters related to the inverse power-law because a limited p_T coverage can not provide a good constraint of the inverse power-law and thus can

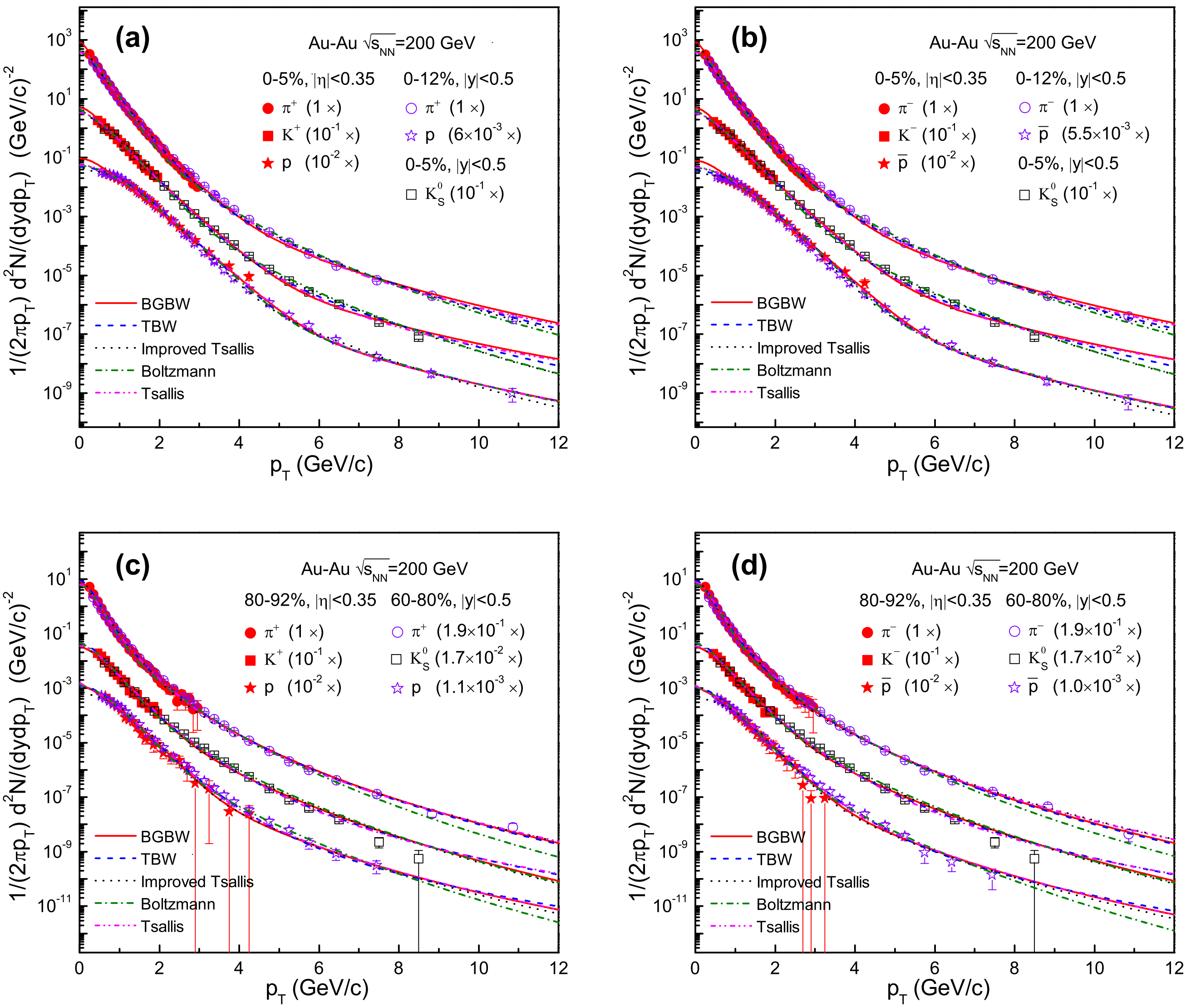

Fig. 1 (Color online) Transverse momentum spectra of (**a**)–(**c**) π^+, K^+, K^0_S, and p, as well as (**b**)–(**d**) π^-, K^-, K^0_S, and $\bar{p}$ produced in (**a**, **b**) central (0–5 and 0–12%) and (**c**, **d**) peripheral (80–92 and 60–80%) Au–Au collisions at $\sqrt{s_{NN}} = 200$ GeV, where the spectra for different types of particles and for the same or similar particles in different conditions are multiplied by different amounts shown in the panels for clarity and normalization. The closed symbols represent the experimental data of the PHENIX Collaboration measured in $|\eta| < 0.35$ [25]. The open symbols represent the STAR data measured in $|y| < 0.5$ [26, 27], where the data for K^+ and K^- are not available and the data for K^0_S in (**a**)–(**c**) and (**b**)–(**d**) are the same. The solid, dashed, dotted, dashed-dotted, and dashed-dotted-dotted curves are our results calculated by using methods (1), (2), (3), (4)$_a$, and (4)$_b$, respectively

easily drive the fitted parameters away from their physical meanings. In fact, for extractions of the effective temperature and transverse flow velocity which are the main topics of the present work, a not too wide p_T coverage, such as 0–2 $\sim$ 3 GeV/c, is enough due to the soft process contributing only in the low p_T region and the changing tendency of data in 0–2 GeV/c that takes part in a main role.

From the above fits one can see that, as a two-component function, Eq. (9) with different soft components can approximately describe the data in a wide p_T coverage. In addition, in our very recent work [37], we used method (3) to describe preliminarily the p_T spectra up to nearly 20 GeV/c. In another work [38], a two-Boltzmann distribution was used to describe the p_T spectra up to nearly 14 GeV/c. Generally, different sets of parameters are needed for different data. In particular, as it is pointed out in Ref. [39], more fitting parameters are needed in order to fit a wider p_T range of particle spectra. In the present work, we fit the particle spectra in a wide p_T range by introducing the inverse power-law to describe the high p_T region. The price to pay is 3 more parameters are added. In the two-component function, the contributions of soft and hard components have little effect in constraining respective free

Table 1 Values of free parameters (T_0, β_T, k, p_0, and n), the normalization constant (N_0), and χ^2/dof corresponding to the fits of method (1) in Figs. 1 and 2, where $n_0 = 2$ in the self-similar flow profile is used as Ref. [11]

Figures	Cent.	Main Part.	T_0 (GeV)	β_T (c)	k	p_0 (GeV/c)	n	N_0	χ^2/dof
1(a)	Central	π^+	0.113 ± 0.004	0.413 ± 0.006	0.988 ± 0.003	2.075 ± 0.062	9.015 ± 0.148	985.309 ± 75.105	2.708
		K^+	0.124 ± 0.005	0.408 ± 0.006	0.975 ± 0.004	1.295 ± 0.058	7.375 ± 0.128	65.180 ± 3.873	7.300
		p	0.127 ± 0.005	0.392 ± 0.006	0.989 ± 0.003	2.485 ± 0.076	8.775 ± 0.136	12.611 ± 0.636	10.729
1(b)	Central	π^-	0.113 ± 0.004	0.413 ± 0.006	0.988 ± 0.003	2.075 ± 0.062	9.015 ± 0.148	985.309 ± 75.105	2.792
		K^-	0.124 ± 0.005	0.408 ± 0.006	0.975 ± 0.004	1.295 ± 0.058	7.375 ± 0.128	63.109 ± 3.589	9.267
		$\bar{p}$	0.125 ± 0.005	0.392 ± 0.006	0.990 ± 0.003	2.465 ± 0.076	8.895 ± 0.136	10.572 ± 0.599	20.512
1(c)	Peripheral	π^+	0.160 ± 0.004	$0.000^{+0.016}_{-0}$	0.754 ± 0.009	2.012 ± 0.069	10.803 ± 0.143	9.794 ± 0.726	4.237
		K^+	0.238 ± 0.005	$0.000^{+0.016}_{-0}$	0.825 ± 0.009	3.383 ± 0.089	12.313 ± 0.166	0.424 ± 0.029	8.755
		p	0.251 ± 0.005	$0.000^{+0.016}_{-0}$	0.851 ± 0.011	2.006 ± 0.065	9.466 ± 0.139	0.167 ± 0.012	1.434
1(d)	Peripheral	π^-	0.160 ± 0.004	$0.000^{+0.016}_{-0}$	0.754 ± 0.009	2.012 ± 0.069	10.803 ± 0.143	9.794 ± 0.726	3.792
		K^-	0.238 ± 0.005	$0.000^{+0.016}_{-0}$	0.825 ± 0.009	3.383 ± 0.089	12.313 ± 0.166	0.424 ± 0.029	7.469
		$\bar{p}$	0.251 ± 0.005	$0.000^{+0.016}_{-0}$	0.851 ± 0.011	2.106 ± 0.066	9.766 ± 0.141	0.134 ± 0.007	0.834
2(a)	Central	π^+	0.128 ± 0.004	0.434 ± 0.007	0.992 ± 0.002	2.775 ± 0.091	7.435 ± 0.133	1771.569 ± 112.825	1.200
		K^+	0.187 ± 0.004	0.390 ± 0.006	0.993 ± 0.002	3.575 ± 0.098	7.135 ± 0.128	92.874 ± 6.429	3.647
		p	0.429 ± 0.005	0.145 ± 0.005	0.976 ± 0.005	2.485 ± 0.088	7.375 ± 0.136	10.188 ± 0.445	7.472
2(b)	Central	π^-	0.128 ± 0.004	0.434 ± 0.007	0.992 ± 0.002	2.775 ± 0.091	7.435 ± 0.133	1771.569 ± 112.825	1.221
		K^-	0.187 ± 0.004	0.390 ± 0.006	0.993 ± 0.002	3.575 ± 0.098	7.135 ± 0.128	92.874 ± 6.429	3.288
		$\bar{p}$	0.428 ± 0.005	0.145 ± 0.005	0.976 ± 0.005	2.485 ± 0.088	7.375 ± 0.136	10.209 ± 0.446	6.875
2(c)	Peripheral	π^+	0.183 ± 0.004	$0.000^{+0.017}_{-0}$	0.909 ± 0.009	2.793 ± 0.089	8.985 ± 0.133	12.144 ± 0.705	16.627
		K^+	0.272 ± 0.004	$0.000^{+0.017}_{-0}$	0.835 ± 0.009	2.375 ± 0.085	7.885 ± 0.165	0.707 ± 0.028	2.808
		p	0.338 ± 0.004	$0.000^{+0.017}_{-0}$	0.836 ± 0.009	1.875 ± 0.078	7.705 ± 0.138	0.183 ± 0.011	2.752
2(d)	Peripheral	π^-	0.183 ± 0.004	$0.000^{+0.017}_{-0}$	0.909 ± 0.009	2.793 ± 0.089	8.985 ± 0.133	12.144 ± 0.705	16.734
		K^-	0.272 ± 0.004	$0.000^{+0.017}_{-0}$	0.835 ± 0.009	2.375 ± 0.085	7.885 ± 0.165	0.707 ± 0.028	3.041
		$\bar{p}$	0.342 ± 0.004	$0.000^{+0.017}_{-0}$	0.815 ± 0.009	1.875 ± 0.078	7.705 ± 0.138	0.185 ± 0.012	2.602

Table 2 Values of free parameters (T_0, q, β_T, k, p_0, and n), the normalization constant (N_0), and χ^2/dof corresponding to the fits of method (2) in Figs. 1 and 2, where $n_0 = 1$ is used as Ref. [14]

Figures	Cent.	Main Part.	T_0 (GeV)	q	β_T (c)	k	p_0 (GeV/c)	n	N_0	χ^2/dof
1(a)	Central	π^+	0.108 ± 0.004	1.008 ± 0.005	0.472 ± 0.010	0.882 ± 0.008	1.775 ± 0.069	9.895 ± 0.143	486.350 ± 40.221	4.082
		K^+	0.113 ± 0.004	1.020 ± 0.005	0.469 ± 0.010	0.901 ± 0.006	1.875 ± 0.072	9.405 ± 0.139	44.575 ± 2.808	6.564
		p	0.119 ± 0.004	1.011 ± 0.004	0.469 ± 0.008	0.989 ± 0.003	2.885 ± 0.082	9.275 ± 0.136	7.214 ± 0.368	1.665
1(b)	Central	π^-	0.108 ± 0.004	1.008 ± 0.005	0.472 ± 0.010	0.882 ± 0.008	1.775 ± 0.069	9.895 ± 0.143	486.350 ± 40.221	3.856
		K^-	0.113 ± 0.004	1.020 ± 0.005	0.469 ± 0.010	0.901 ± 0.006	1.875 ± 0.072	9.405 ± 0.139	42.837 ± 2.808	5.939
		$\bar{p}$	0.121 ± 0.004	1.010 ± 0.004	0.469 ± 0.008	0.991 ± 0.003	2.885 ± 0.082	9.305 ± 0.134	5.369 ± 0.354	6.643
1(c)	Peripheral	π^+	0.099 ± 0.004	1.078 ± 0.005	$0.000^{+0.036}_{-0}$	0.862 ± 0.008	2.198 ± 0.089	10.982 ± 0.161	11.341 ± 0.747	3.221
		K^+	0.119 ± 0.004	1.088 ± 0.004	$0.000^{+0.036}_{-0}$	0.985 ± 0.008	1.983 ± 0.078	8.253 ± 0.138	0.589 ± 0.053	4.002
		p	0.132 ± 0.004	1.064 ± 0.005	$0.000^{+0.036}_{-0}$	0.985 ± 0.004	2.010 ± 0.088	7.966 ± 0.129	0.171 ± 0.014	0.940
1(d)	Peripheral	π^-	0.099 ± 0.004	1.078 ± 0.005	$0.000^{+0.036}_{-0}$	0.862 ± 0.008	2.198 ± 0.089	10.982 ± 0.161	11.341 ± 0.747	2.924
		K^-	0.119 ± 0.004	1.088 ± 0.004	$0.000^{+0.036}_{-0}$	0.985 ± 0.008	1.983 ± 0.078	8.253 ± 0.138	0.589 ± 0.053	3.652
		$\bar{p}$	0.124 ± 0.004	1.067 ± 0.005	$0.000^{+0.036}_{-0}$	0.983 ± 0.004	2.018 ± 0.088	8.166 ± 0.129	0.144 ± 0.014	0.552
2(a)	Central	π^+	0.109 ± 0.004	1.009 ± 0.005	0.525 ± 0.009	0.977 ± 0.005	2.585 ± 0.086	7.875 ± 0.122	917.576 ± 91.809	6.313
		K^+	0.145 ± 0.005	1.004 ± 0.003	0.500 ± 0.009	0.984 ± 0.004	3.255 ± 0.091	7.508 ± 0.119	66.904 ± 6.743	0.580
		p	0.178 ± 0.005	1.002 ± 0.001	0.500 ± 0.008	0.993 ± 0.002	4.975 ± 0.099	8.725 ± 0.121	8.981 ± 0.254	3.509
2(b)	Central	π^-	0.109 ± 0.004	1.009 ± 0.005	0.525 ± 0.009	0.977 ± 0.005	2.585 ± 0.086	7.875 ± 0.122	917.576 ± 91.809	6.249
		K^-	0.145 ± 0.005	1.004 ± 0.003	0.500 ± 0.009	0.985 ± 0.004	3.255 ± 0.091	7.508 ± 0.119	66.904 ± 6.743	0.570
		$\bar{p}$	0.178 ± 0.005	1.002 ± 0.001	0.500 ± 0.008	0.993 ± 0.002	4.975 ± 0.099	8.725 ± 0.121	8.981 ± 0.254	3.253
2(c)	Peripheral	π^+	0.102 ± 0.004	1.108 ± 0.005	$0.000^{+0.018}_{-0}$	0.976 ± 0.005	3.003 ± 0.089	8.335 ± 0.118	15.628 ± 0.563	10.532
		K^+	0.141 ± 0.005	1.099 ± 0.005	$0.000^{+0.018}_{-0}$	0.906 ± 0.005	1.875 ± 0.071	7.038 ± 0.109	0.820 ± 0.063	1.149
		p	0.172 ± 0.005	1.076 ± 0.005	$0.000^{+0.018}_{-0}$	0.958 ± 0.005	2.375 ± 0.088	7.575 ± 0.119	0.212 ± 0.017	4.623
2(d)	Peripheral	π^-	0.102 ± 0.004	1.108 ± 0.005	$0.000^{+0.018}_{-0}$	0.976 ± 0.005	3.003 ± 0.089	8.335 ± 0.118	15.628 ± 0.563	10.481
		K^-	0.141 ± 0.005	1.099 ± 0.005	$0.000^{+0.018}_{-0}$	0.906 ± 0.005	1.875 ± 0.071	7.038 ± 0.109	0.820 ± 0.063	1.279
		$\bar{p}$	0.172 ± 0.005	1.076 ± 0.005	$0.000^{+0.018}_{-0}$	0.958 ± 0.005	2.375 ± 0.088	7.575 ± 0.119	0.212 ± 0.017	4.832

Table 3 Values of free parameters (T_0, q, β_T, k, p_0, and n), the normalization constant (N_0), and χ^2/dof corresponding to the fits of method (3) in Figs. 1 and 2

Figures	Cent.	Main Part.	T_0 (GeV)	q	β_T (c)	k	p_0 (GeV/c)	n	N_0	χ^2/dof
1(a)	Central	π^+	0.113 ± 0.006	1.017 ± 0.007	0.634 ± 0.009	0.939 ± 0.008	2.475 ± 0.088	11.091 ± 0.165	746.564 ± 89.743	2.986
		K^+	0.116 ± 0.006	1.040 ± 0.007	0.634 ± 0.009	0.902 ± 0.008	3.675 ± 0.091	12.995 ± 0.172	32.457 ± 5.734	9.781
		p	0.121 ± 0.006	1.024 ± 0.007	0.634 ± 0.009	0.916 ± 0.008	2.985 ± 0.090	11.225 ± 0.162	5.365 ± 0.677	1.249
1(b)	Central	π^-	0.113 ± 0.006	1.017 ± 0.007	0.634 ± 0.009	0.939 ± 0.008	2.475 ± 0.088	11.091 ± 0.165	746.564 ± 89.743	2.700
		K^-	0.116 ± 0.006	1.040 ± 0.007	0.634 ± 0.009	0.900 ± 0.008	3.675 ± 0.091	12.995 ± 0.172	31.193 ± 5.698	8.100
		$\bar{p}$	0.121 ± 0.006	1.024 ± 0.007	0.634 ± 0.009	0.909 ± 0.008	2.985 ± 0.090	11.525 ± 0.162	8.294 ± 1.243	2.878
1(c)	Peripheral	π^+	0.102 ± 0.006	1.031 ± 0.007	0.583 ± 0.009	0.891 ± 0.008	2.185 ± 0.086	10.632 ± 0.148	10.292 ± 1.860	3.931
		K^+	0.109 ± 0.006	1.045 ± 0.008	0.578 ± 0.009	0.872 ± 0.008	4.483 ± 0.099	14.061 ± 0.165	0.327 ± 0.057	8.529
		p	0.110 ± 0.006	1.053 ± 0.008	0.548 ± 0.008	0.901 ± 0.008	3.066 ± 0.095	11.166 ± 0.126	0.083 ± 0.005	2.700
1(d)	Peripheral	π^-	0.102 ± 0.006	1.031 ± 0.007	0.583 ± 0.009	0.891 ± 0.008	2.185 ± 0.086	10.532 ± 0.148	10.771 ± 1.863	3.751
		K^-	0.109 ± 0.006	1.045 ± 0.008	0.578 ± 0.009	0.872 ± 0.008	4.483 ± 0.099	14.061 ± 0.165	0.327 ± 0.057	7.157
		$\bar{p}$	0.110 ± 0.006	1.053 ± 0.008	0.548 ± 0.008	0.901 ± 0.008	3.066 ± 0.095	11.166 ± 0.126	0.055 ± 0.005	1.316
2(a)	Central	π^+	0.152 ± 0.004	1.011 ± 0.004	0.609 ± 0.010	0.981 ± 0.007	2.575 ± 0.094	7.775 ± 0.145	1475.441 ± 93.801	2.682
		K^+	0.158 ± 0.004	1.059 ± 0.008	0.609 ± 0.010	0.987 ± 0.006	3.575 ± 0.102	7.655 ± 0.144	58.904 ± 5.207	1.235
		p	0.194 ± 0.005	1.069 ± 0.011	0.609 ± 0.010	0.987 ± 0.006	2.885 ± 0.101	7.375 ± 0.148	7.792 ± 0.559	4.833
2(b)	Central	π^-	0.152 ± 0.004	1.011 ± 0.004	0.609 ± 0.010	0.981 ± 0.007	2.575 ± 0.094	7.775 ± 0.145	1475.441 ± 93.801	2.586
		K^-	0.158 ± 0.004	1.059 ± 0.008	0.609 ± 0.010	0.987 ± 0.006	3.575 ± 0.102	7.655 ± 0.144	58.904 ± 5.207	1.083
		$\bar{p}$	0.194 ± 0.005	1.069 ± 0.011	0.609 ± 0.010	0.987 ± 0.006	2.885 ± 0.101	7.375 ± 0.148	7.792 ± 0.559	4.482
2(c)	Peripheral	π^+	0.118 ± 0.005	1.008 ± 0.005	0.630 ± 0.009	0.920 ± 0.007	2.903 ± 0.103	9.135 ± 0.165	15.956 ± 0.981	5.202
		K^+	0.143 ± 0.004	1.011 ± 0.005	0.602 ± 0.009	0.901 ± 0.007	3.003 ± 0.111	8.335 ± 0.155	0.530 ± 0.038	1.880
		p	0.163 ± 0.005	1.021 ± 0.005	0.559 ± 0.009	0.889 ± 0.007	2.375 ± 0.099	8.059 ± 0.142	0.102 ± 0.006	2.804
2(d)	Peripheral	π^-	0.118 ± 0.005	1.008 ± 0.005	0.630 ± 0.009	0.920 ± 0.007	2.903 ± 0.103	9.135 ± 0.165	15.956 ± 0.981	5.257
		K^-	0.143 ± 0.004	1.011 ± 0.005	0.602 ± 0.009	0.901 ± 0.007	3.003 ± 0.111	8.335 ± 0.155	0.525 ± 0.034	1.979
		$\bar{p}$	0.163 ± 0.005	1.021 ± 0.005	0.559 ± 0.009	0.889 ± 0.007	2.375 ± 0.099	8.059 ± 0.142	0.101 ± 0.006	2.942

Table 4 Values of free parameters (T, k, p_0, and n), the normalization constant (N_0), and χ^2/dof corresponding to the fits of method $(4)_a$ in Figs. 1 and 2

Figures	Cent.	Main Part.	T (GeV)	k	p_0 (GeV/c)	n	N_0	χ^2/dof
1(a)	Central	π^+	0.167 ± 0.004	0.765 ± 0.008	2.095 ± 0.068	11.295 ± 0.133	519.268 ± 39.582	9.637
		K^+	0.235 ± 0.004	0.752 ± 0.008	2.915 ± 0.068	12.335 ± 0.185	49.650 ± 2.890	12.847
		p	0.302 ± 0.005	0.983 ± 0.005	2.785 ± 0.066	9.475 ± 0.176	7.744 ± 0.267	2.217
1(b)	Central	π^-	0.167 ± 0.004	0.765 ± 0.008	2.095 ± 0.068	11.295 ± 0.133	519.297 ± 39.582	9.068
		K^-	0.235 ± 0.004	0.750 ± 0.008	2.915 ± 0.068	12.335 ± 0.185	47.297 ± 2.893	13.624
		$\bar{p}$	0.296 ± 0.005	0.981 ± 0.005	2.715 ± 0.066	9.675 ± 0.176	6.516 ± 0.272	6.399
1(c)	Peripheral	π^+	0.131 ± 0.004	0.799 ± 0.008	3.238 ± 0.089	13.892 ± 0.132	8.602 ± 0.676	4.243
		K^+	0.185 ± 0.004	0.702 ± 0.008	3.483 ± 0.086	13.083 ± 0.146	0.556 ± 0.035	6.799
		p	0.209 ± 0.005	0.822 ± 0.008	4.606 ± 0.106	14.866 ± 0.155	0.173 ± 0.012	0.955
1(d)	Peripheral	π^-	0.131 ± 0.004	0.799 ± 0.008	3.238 ± 0.089	13.892 ± 0.132	8.602 ± 0.676	4.115
		K^-	0.185 ± 0.004	0.702 ± 0.008	3.483 ± 0.086	13.083 ± 0.146	0.559 ± 0.035	6.284
		$\bar{p}$	0.209 ± 0.005	0.822 ± 0.008	4.606 ± 0.106	15.279 ± 0.165	0.139 ± 0.012	0.627
2(a)	Central	π^+	0.215 ± 0.004	0.828 ± 0.008	1.375 ± 0.068	7.315 ± 0.128	679.491 ± 44.189	16.706
		K^+	0.299 ± 0.005	0.972 ± 0.008	2.945 ± 0.090	7.685 ± 0.132	57.722 ± 5.536	1.889
		p	0.413 ± 0.005	0.993 ± 0.002	4.975 ± 0.112	8.725 ± 0.146	8.864 ± 0.467	2.600
2(b)	Central	π^-	0.215 ± 0.004	0.828 ± 0.008	1.375 ± 0.068	7.315 ± 0.128	679.491 ± 44.189	16.821
		K^-	0.299 ± 0.005	0.972 ± 0.008	2.945 ± 0.090	7.685 ± 0.132	57.722 ± 5.536	2.052
		$\bar{p}$	0.413 ± 0.005	0.993 ± 0.002	4.975 ± 0.112	8.725 ± 0.146	8.864 ± 0.467	2.433
2(c)	Peripheral	π^+	0.152 ± 0.004	0.802 ± 0.008	2.012 ± 0.065	8.279 ± 0.116	9.713 ± 0.616	15.656
		K^+	0.219 ± 0.004	0.803 ± 0.009	2.035 ± 0.092	7.595 ± 0.134	0.822 ± 0.052	5.123
		p	0.291 ± 0.005	0.805 ± 0.008	2.285 ± 0.096	8.365 ± 0.142	0.190 ± 0.017	3.545
2(d)	Peripheral	π^-	0.152 ± 0.004	0.802 ± 0.008	2.012 ± 0.065	8.279 ± 0.116	9.713 ± 0.616	15.657
		K^-	0.219 ± 0.004	0.803 ± 0.009	2.035 ± 0.092	7.595 ± 0.134	0.822 ± 0.052	5.238
		$\bar{p}$	0.296 ± 0.005	0.805 ± 0.008	2.285 ± 0.096	8.365 ± 0.142	0.188 ± 0.017	3.391

parameters due to different contributive regions, though the contribution fraction of the two components is the main role. This results in the p_T coverage having a small effect on T_0 and β_T. In fact, if we change the boundary of the low p_T region from 2 to 3 or 3.5 GeV/c, the variations of parameters can be neglected due to the tendency of the curve being mainly determined by the data in 0–2 GeV/c. Meanwhile, the data in 2–3.5 GeV/c obey naturally the tendency of the curve due to also the contribution or revision of the hard component. In other words, because of the revision of the hard component, the values of T_0 and β_T are not sensitive to the boundary of low p_T region. Although different p_T coverages obtained in different conditions can drive different fitted curves, these differences appear mainly in the high p_T region and do not largely effect the extraction of T_0 and β_T. In any case, we always use the last square method to extract the fitted parameters. In fact, the method used by us has the minimum randomness in the extractions of the fitted parameters.

It should be noted that although the conventional BGBW and TBW models have only 2–3 parameters to describe the p_T shape and usually fit several spectra simultaneously to reduce the correlation of the parameters, they seem to cover non-simultaneity of the kinetic freeze-outs of different particles. In the present work, although we use 3 more parameters to fit each spectrum individually, we observe an evidence of the mass dependent differential kinetic freeze-out scenario or multiple kinetic freeze-outs scenario [4, 16, 23]. The larger the temperature (mass) is, the earlier the particle produces. The average temperature (flow velocity and entropy index) of the kinetic freeze-outs for different particles is obtained by weighing different T_0 (β_T and q), where the weight factor is the normalization constant of each p_T spectrum. In the case of using the average temperature (flow velocity and entropy index) to fit the pion, kaon, and proton simultaneously to better constrain the parameters, larger values of χ^2/dof are obtained.

Based on the descriptions of the p_T spectra, the first three methods can get T_0 and β_T, though the values of parameters are possibly inharmonious due to different

Table 5 Values of free parameters (T, q, k, p_0, and n), the normalization constant (N_0), and χ^2/dof corresponding to the fits of method $(4)_b$ in Figs. 1 and 2

Figures	Cent.	Main Part.	T (GeV)	q	k	p_0 (GeV/c)	n	N_0	χ^2/dof
1(a)	Central	π^+	0.130 ± 0.004	1.073 ± 0.003	0.994 ± 0.003	1.775 ± 0.069	8.115 ± 0.148	508.830 ± 43.650	1.731
		K^+	0.184 ± 0.005	1.050 ± 0.004	0.984 ± 0.005	1.075 ± 0.058	6.775 ± 0.135	45.687 ± 2.962	4.354
		p	0.274 ± 0.004	1.015 ± 0.003	0.988 ± 0.003	2.485 ± 0.088	8.775 ± 0.152	8.211 ± 0.194	3.268
1(b)	Central	π^-	0.130 ± 0.004	1.073 ± 0.003	0.994 ± 0.003	1.775 ± 0.069	8.115 ± 0.148	508.830 ± 43.650	1.648
		K^-	0.184 ± 0.005	1.050 ± 0.004	0.982 ± 0.005	1.075 ± 0.058	6.775 ± 0.135	42.366 ± 2.868	2.951
		$\bar{p}$	0.272 ± 0.004	1.012 ± 0.003	0.992 ± 0.003	2.985 ± 0.090	9.375 ± 0.159	6.764 ± 0.189	7.806
1(c)	Peripheral	π^+	0.105 ± 0.004	1.085 ± 0.005	0.918 ± 0.005	1.985 ± 0.075	10.032 ± 0.155	8.344 ± 0.606	1.855
		K^+	0.137 ± 0.004	1.079 ± 0.004	0.990 ± 0.006	1.983 ± 0.075	7.853 ± 0.136	0.488 ± 0.033	3.574
		p	0.192 ± 0.005	1.028 ± 0.006	0.853 ± 0.008	2.006 ± 0.056	9.466 ± 0.155	0.175 ± 0.012	1.165
1(d)	Peripheral	π^-	0.105 ± 0.004	1.085 ± 0.005	0.918 ± 0.005	1.985 ± 0.075	10.032 ± 0.155	8.344 ± 0.606	1.635
		K^-	0.137 ± 0.004	1.079 ± 0.004	0.990 ± 0.006	1.983 ± 0.075	7.853 ± 0.136	0.466 ± 0.030	2.604
		$\bar{p}$	0.192 ± 0.005	1.028 ± 0.006	0.853 ± 0.008	2.106 ± 0.059	9.766 ± 0.158	0.140 ± 0.012	0.715
2(a)	Central	π^+	0.170 ± 0.005	1.066 ± 0.005	0.992 ± 0.007	2.775 ± 0.062	7.275 ± 0.185	711.631 ± 55.063	6.847
		K^+	0.264 ± 0.006	1.030 ± 0.005	0.993 ± 0.002	3.575 ± 0.108	7.135 ± 0.203	62.036 ± 5.422	0.548
		p	0.409 ± 0.006	1.002 ± 0.001	0.993 ± 0.002	4.975 ± 0.112	8.725 ± 0.206	8.968 ± 0.417	2.813
2(b)	Central	π^-	0.170 ± 0.005	1.066 ± 0.005	0.992 ± 0.007	2.775 ± 0.062	7.275 ± 0.185	711.631 ± 55.063	6.813
		K^-	0.264 ± 0.006	1.030 ± 0.005	0.993 ± 0.002	3.575 ± 0.108	7.135 ± 0.203	62.036 ± 5.422	0.654
		$\bar{p}$	0.409 ± 0.006	1.002 ± 0.001	0.993 ± 0.002	4.975 ± 0.112	8.725 ± 0.206	8.968 ± 0.417	2.651
2(c)	Peripheral	π^+	0.117 ± 0.004	1.099 ± 0.005	0.972 ± 0.005	3.003 ± 0.098	8.335 ± 0.196	10.635 ± 0.595	7.995
		K^+	0.173 ± 0.005	1.069 ± 0.005	0.905 ± 0.006	2.375 ± 0.071	7.575 ± 0.192	0.725 ± 0.043	1.674
		p	0.263 ± 0.005	1.035 ± 0.005	0.911 ± 0.006	1.875 ± 0.065	7.265 ± 0.146	0.139 ± 0.009	2.285
2(d)	Peripheral	π^-	0.117 ± 0.004	1.099 ± 0.005	0.972 ± 0.005	3.003 ± 0.098	8.335 ± 0.196	10.635 ± 0.595	7.904
		K^-	0.173 ± 0.005	1.069 ± 0.005	0.905 ± 0.006	2.375 ± 0.071	7.575 ± 0.192	0.725 ± 0.043	1.875
		$\bar{p}$	0.263 ± 0.005	1.035 ± 0.005	0.911 ± 0.006	1.875 ± 0.065	7.265 ± 0.146	0.144 ± 0.009	2.255

methods. In particular, the value of T_0 obtained by method (1) in peripheral collisions is larger than that in central collisions, which is different from methods (2) and (3) which obtain an opposite result. According to the conventional treatment in Refs. [11, 14], the values of β_T obtained by methods (1) and (2) in peripheral collisions are taken to be nearly zero, which are different from method (3) which obtains a value of about 0.6c in both central and peripheral collisions.

To obtain the values of T_0, β_T, and β by methods $(4)_a$ and $(4)_b$, we analyze the values of T presented in Tables 4 and 5, and calculate $\langle p_T \rangle$, $\langle p \rangle$, and $\overline{m}$ based on the values of parameters listed in Tables 4 and 5. In the calculations performed from p_T to $\langle p \rangle$ and $\overline{m}$ by the Monte Carlo method, an isotropic assumption in the rest frame of emission source is used [22–24]. In particular, $\overline{m}$ is in fact the mean energy, $\langle \sqrt{p^2 + m_0^2} \rangle$.

The relations between T and m_0, $\langle p_T \rangle$ and $\overline{m}$, as well as $\langle p \rangle$ and $\overline{m}$ are shown in Figs. 3, 4 and 5, respectively, where panels (a) and (b) correspond to methods $(4)_a$ and $(4)_b$ which use the Boltzmann and Tsallis distributions, respectively. Different symbols represent central (0–5 and 0–12%) and peripheral (80–92 and 60–80%) Au–Au collisions at $\sqrt{s_{NN}} = 200$ GeV and central (0–5%) and peripheral (80–90 and 60–80%) Pb–Pb collisions at $\sqrt{s_{NN}} = 2.76$ TeV respectively, where the centralities 0–5 and 0–12%, 80–92 and 60–80%, as well as 80–90 and 60–80% can be combined to 0–12, 60–92, and 60–90%, respectively. The symbols in Fig. 3 represent values of T listed in Tables 4 and 5 for a different m_0. The symbols in Figs. 4 and 5 represent values of $\langle p_T \rangle$ and $\langle p \rangle$ for different $\overline{m}$ respectively, which are calculated due to the parameters listed in Tables 4 and 5 and the isotropic assumption in the rest frame of the emission source. The solid and dashed lines in the three figures are the results fitted by the least square method for the positively and negatively charged particles, respectively. The values of intercepts, slopes, and χ^2/dof are listed in Tables 6 and 7 which correspond to methods $(4)_a$ and $(4)_b$ respectively. One can see that, in most cases, the mentioned relations are described by a

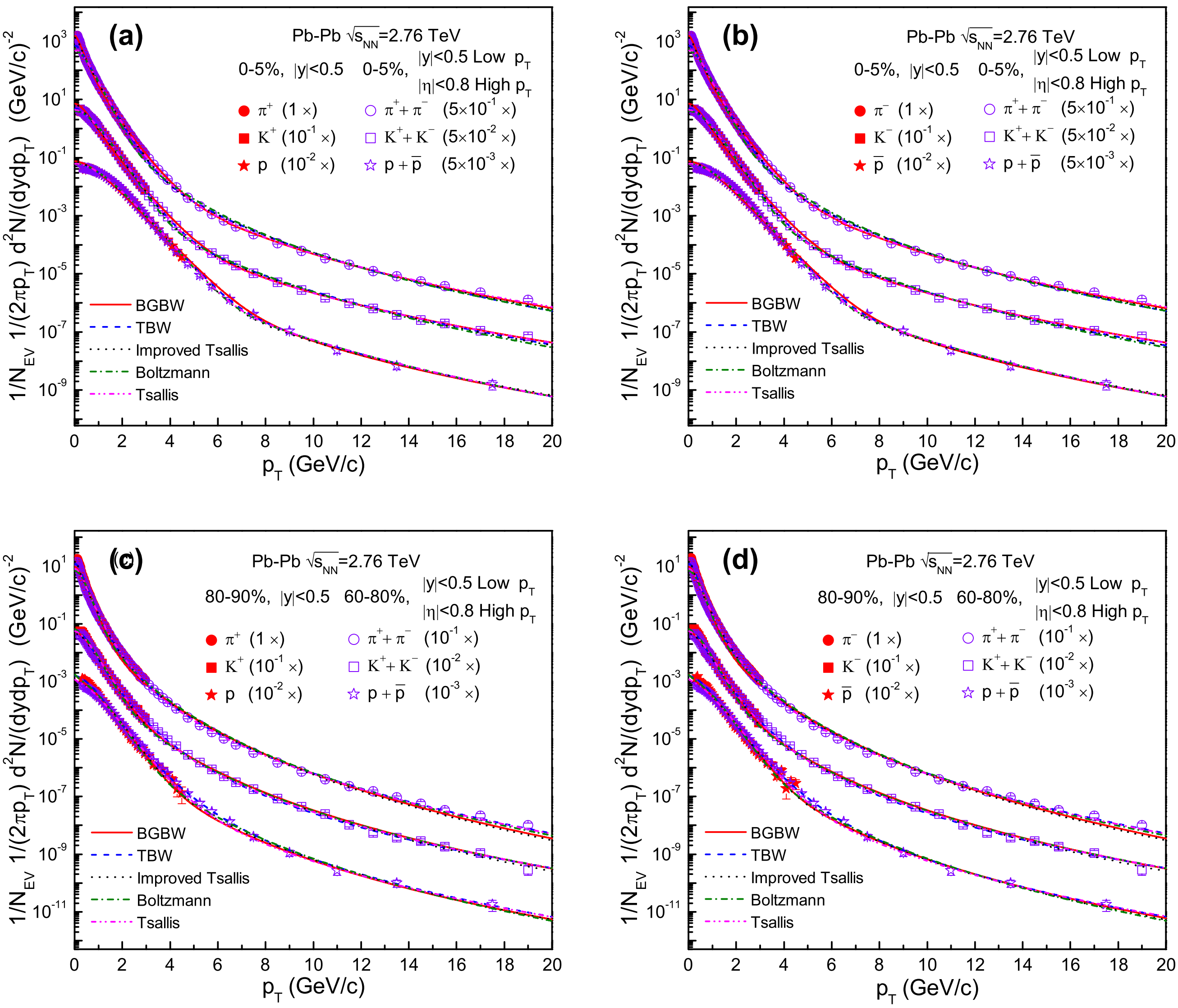

Fig. 2 (Color online) Same as Fig. 1, but showing the spectra of (**a**)–(**c**) π^+ ($\pi^+ + \pi^-$), K^+ ($K^+ + K^-$), and p ($p + \bar{p}$), as well as (**b**)–(**d**) π^- ($\pi^+ + \pi^-$), K^- ($K^+ + K^-$), and $\bar{p}$ ($p + \bar{p}$) produced in (**a**, **b**) central (0–5%) and (**c**, **d**) peripheral (80–90 and 60–80%) Pb–Pb collisions at $\sqrt{s_{NN}} = 2.76$ TeV, where N_{EV} on the vertical axis denotes the number of events, which is usually omitted. The closed (open) symbols represent the experimental data of the ALICE Collaboration measured in $|y| < 0.5$ [28] (in $|\eta| < 0.8$ for high p_T region and in $|y| < 0.5$ for low p_T region [29]). The data for $\pi^+ + \pi^-$, $K^+ + K^-$, and $p + \bar{p}$ in (**a**)–(**c**) and (**b**)–(**d**) are the same

linear function. In particular, the intercept in Fig. 3 is regarded as T_0, and the slopes in Figs. 4 and 5 are regarded as β_T and β, respectively. The values of T, T_0, β_T, β, and $\overline{m}$ are approximately independent of isospin.

To compare the values of key parameters obtained by different methods for different centralities (both central and peripheral collisions), Figs. 6 and 7 show T_0 and β_T respectively, where panels (a) and (b) correspond to the results for central (0–5 and 0–12%) and peripheral (80–92 and 60–80%) Au–Au collisions at $\sqrt{s_{NN}} = 200$ GeV and central (0–5%) and peripheral (80–90 and 60–80%) Pb–Pb collisions at $\sqrt{s_{NN}} = 2.76$ TeV, respectively. The closed and open symbols represent positively and negatively charged particles respectively, which are quoted from Tables 1, 2, 3, 6 and 7 which correspond to methods (1), (2), (3), $(4)_a$, and $(4)_b$, respectively. In particular, the values of T_0 and β_T in the first three methods are obtained by weighing different particles. One can see that, by using method (1), the value of T_0 in central collisions is smaller than that in peripheral collisions, and other methods present a larger T_0 in central collisions. Methods (1) and (2) show a nearly zero β_T in peripheral collisions according to Refs. [11, 14], while other methods show a considerable β_T in both central and peripheral collisions.

To explain the inconsistent results in T_0 and β_T for different methods, we re-examine the first two methods. It

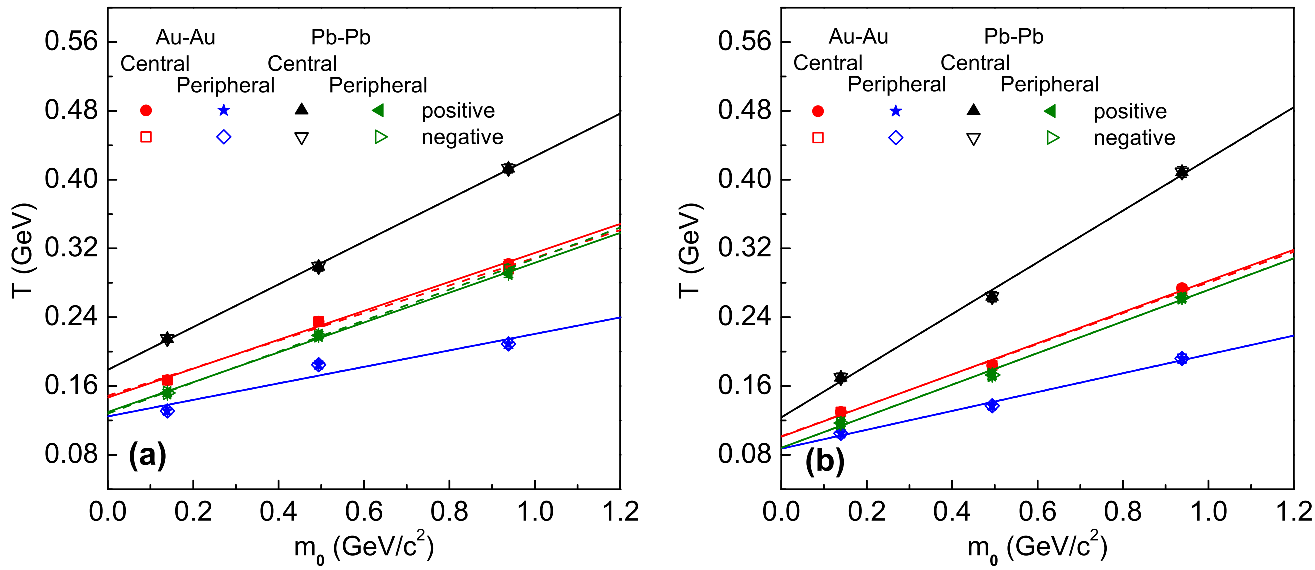

Fig. 3 (Color online) Relations between T and m_0. Different symbols represent central (0–5 and 0–12%) and peripheral (80–92 and 60–80%) Au–Au collisions at $\sqrt{s_{\mathrm{NN}}} = 200$ GeV and central (0–5%) and peripheral (80–90 and 60–80%) Pb–Pb collisions at $\sqrt{s_{\mathrm{NN}}} = 2.76$ TeV respectively. The symbols presented in panels (**a**) and (**b**) represent the results listed in Tables 4 and 5 and correspond to the fits of Boltzmann and Tsallis distributions, respectively, where the closed and open symbols show the results of positively and negatively charged particles respectively. The solid and dashed lines are the results fitted by the least square method for the positively and negatively charged particles respectively, where the intercepts are regarded as T_0

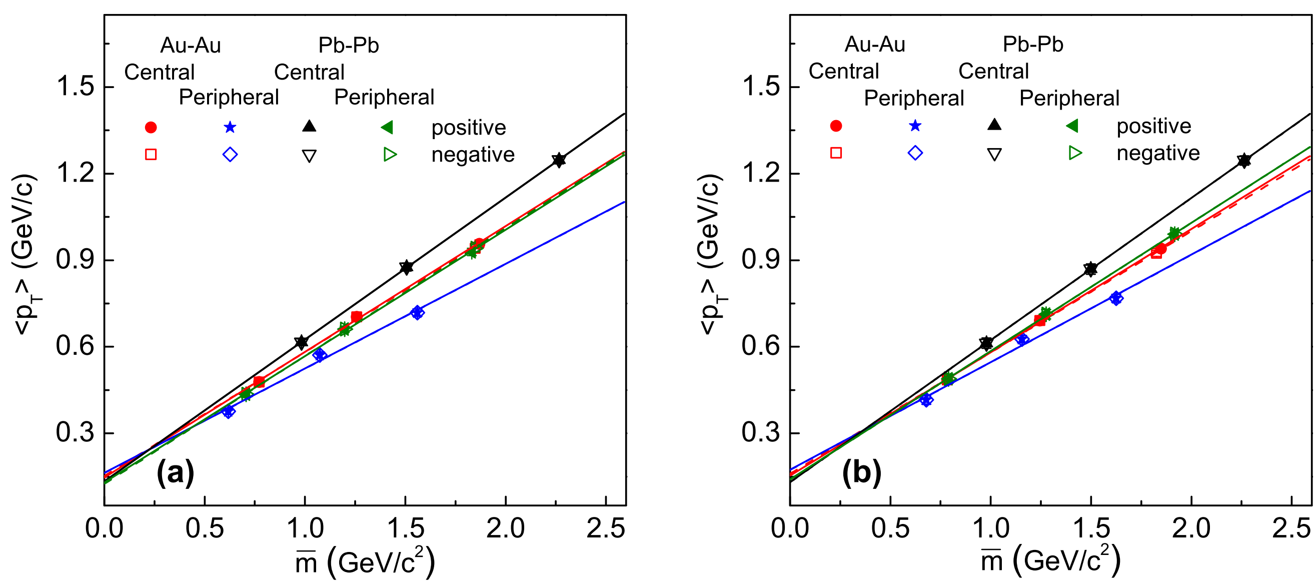

Fig. 4 (Color online) Same as Fig. 3, but showing the relations between $\langle p_T \rangle$ and $\overline{m}$, and the slopes are regarded as β_T. The symbols presented in panels (**a**) and (**b**) represent the results obtained according to the fits of Boltzmann and Tsallis distributions, respectively, where the values of parameters are listed in Tables 4 and 5, respectively

should be noticed that the same flow profile function, $\beta(r) = \beta_S (r/R)^{n_0}$, and the same transverse flow velocity, $\beta_T = 2\beta_S/(n_0 + 2)$, are used in the first two methods, though $n_0 = 2$ is used in method (1) [11] and $n_0 = 1$ is used in method (2) [14] with the conventional treatment. As an insensitive quantity, although the radial size R of the thermal source in central collisions can be approximately regarded as the radius of a collision nucleus and in peripheral collisions R is not zero due to a few participant nucleons taking part in the interactions in which we can take approximate R to be 2.5 fm, both methods (1) and (2) use a nearly zero β_T in peripheral collisions [11, 14]. If we consider a non-zero β_T in peripheral collisions for methods (1) and (2), the situation will be changed.

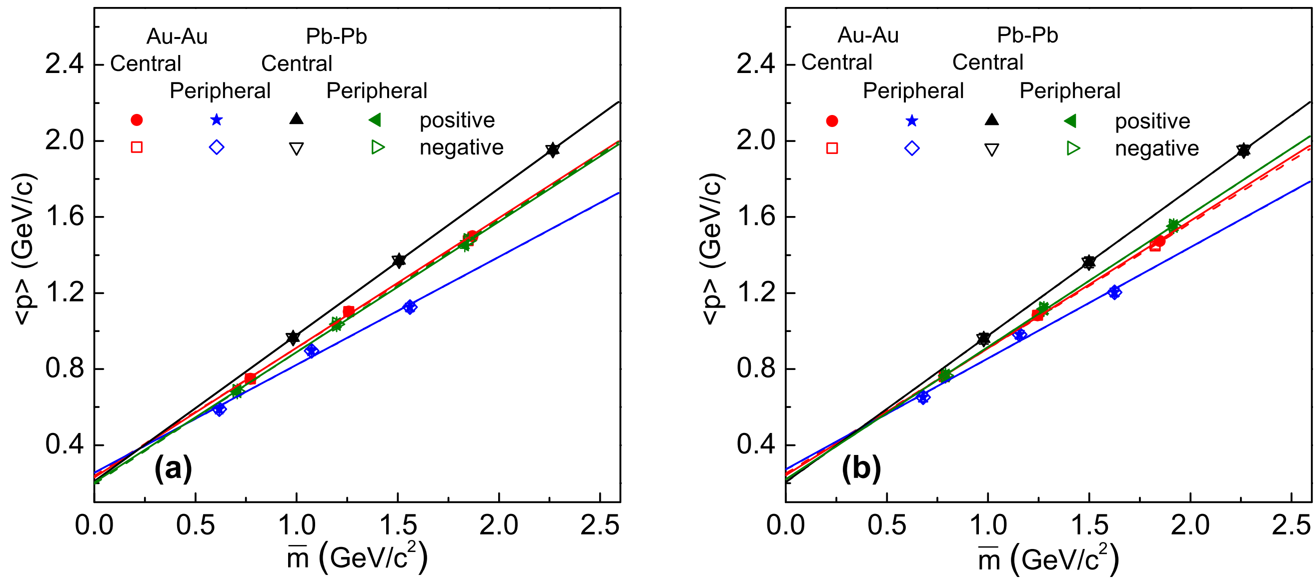

Fig. 5 (Color online) Same as Fig. 3, but showing the relations between $\langle p \rangle$ and $\overline{m}$, and the slopes are regarded as β. The symbols presented in panels (**a**) and (**b**) represent the results obtained according to the fits of Boltzmann and Tsallis distributions, respectively, where the values of parameters are listed in Tables 4 and 5 respectively

Table 6 Values of free parameters (intercept and slope) and χ^2/dof corresponding to the relations obtained from the fits of the Boltzmann distribution in Figs. 3a, 4a and 5a

Figures	Relation	Type and main particles	Centrality	Intercept	Slope	χ^2/dof
3(a)	$T - m_0$	Au–Au positive	Central	0.147 ± 0.007	0.168 ± 0.012	2.625
		Negative	Central	0.149 ± 0.010	0.160 ± 0.016	4.618
		Positive	Peripheral	0.125 ± 0.017	0.096 ± 0.028	14.910
		Negative	Peripheral	0.125 ± 0.017	0.096 ± 0.028	14.910
		Pb–Pb positive	Central	0.179 ± 0.003	0.248 ± 0.005	0.424
		Negative	Central	0.179 ± 0.003	0.248 ± 0.005	0.424
		Positive	Peripheral	0.130 ± 0.005	0.174 ± 0.008	1.142
		Negative	Peripheral	0.128 ± 0.003	0.180 ± 0.005	0.394
4(a)	$\langle p_T \rangle - \overline{m}$	Au–Au positive	Central	0.147 ± 0.018	0.436 ± 0.013	0.864
		Negative	Central	0.152 ± 0.023	0.430 ± 0.017	1.312
		Positive	Peripheral	0.163 ± 0.041	0.362 ± 0.036	4.734
		Negative	Peripheral	0.163 ± 0.041	0.362 ± 0.036	4.734
		Pb–Pb positive	Central	0.133 ± 0.004	0.492 ± 0.002	0.024
		Negative	Central	0.133 ± 0.004	0.492 ± 0.002	0.024
		Positive	Peripheral	0.130 ± 0.013	0.438 ± 0.010	0.499
		Negative	Peripheral	0.125 ± 0.010	0.443 ± 0.007	0.285
5(a)	$\langle p \rangle - \overline{m}$	Au–Au positive	Central	0.230 ± 0.028	0.683 ± 0.021	0.865
		Negative	Central	0.239 ± 0.035	0.673 ± 0.026	1.313
		Positive	Peripheral	0.255 ± 0.064	0.568 ± 0.056	4.746
		Negative	Peripheral	0.255 ± 0.064	0.568 ± 0.056	4.746
		Pb–Pb Positive	Central	0.209 ± 0.006	0.771 ± 0.003	0.024
		Negative	Central	0.209 ± 0.006	0.771 ± 0.003	0.024
		Positive	Peripheral	0.203 ± 0.020	0.686 ± 0.015	0.496
		Negative	Peripheral	0.196 ± 0.015	0.694 ± 0.011	0.283

By using a non-zero β_T in peripheral collisions for methods (1) and (2), we re-analyze the data presented in Figs. 1 and 2. At the same time, to see the influences of different n_0 in the self-similar flow profile, we refit the mentioned p_T spectra by the first two methods with $n_0 = 1$ and 2 synchronously. The results re-analyzed by us are

Table 7 Values of free parameters (intercept and slope) and χ^2/dof corresponding to the relations obtained from the fits of the Tsallis distribution in Figs. 3b, 4b and 5b

Figures	Relation	Type and main particles	Centrality	Intercept	Slope	χ^2/dof
3(b)	$T - m_0$	Au–Au positive	Central	0.101 ± 0.009	0.181 ± 0.014	3.059
		Negative	Central	0.102 ± 0.008	0.179 ± 0.013	2.533
		Positive	Peripheral	0.087 ± 0.006	0.110 ± 0.009	1.708
		Negative	Peripheral	0.087 ± 0.006	0.110 ± 0.009	1.708
		Pb–Pb positive	Central	0.124 ± 0.011	0.300 ± 0.017	2.877
		Negative	Central	0.124 ± 0.011	0.300 ± 0.017	2.877
		Positive	Peripheral	0.088 ± 0.008	0.184 ± 0.013	2.258
		Negative	Peripheral	0.088 ± 0.008	0.184 ± 0.013	2.258
4(b)	$\langle p_T \rangle - \overline{m}$	Au–Au positive	Central	0.154 ± 0.013	0.427 ± 0.010	0.270
		Negative	Central	0.160 ± 0.018	0.420 ± 0.013	0.495
		Positive	Peripheral	0.174 ± 0.049	0.373 ± 0.040	4.116
		Negative	Peripheral	0.174 ± 0.049	0.373 ± 0.040	4.116
		Pb–Pb positive	Central	0.131 ± 0.001	0.493 ± 0.001	0.001
		Negative	Central	0.131 ± 0.001	0.493 ± 0.001	0.001
		Positive	Peripheral	0.140 ± 0.011	0.445 ± 0.008	0.148
		Negative	Peripheral	0.140 ± 0.011	0.445 ± 0.008	0.148
5(b)	$\langle p \rangle - \overline{m}$	Au–Au positive	Central	0.240 ± 0.021	0.670 ± 0.015	0.269
		Negative	Central	0.251 ± 0.028	0.659 ± 0.021	0.494
		Positive	Peripheral	0.272 ± 0.077	0.584 ± 0.063	4.111
		Negative	Peripheral	0.272 ± 0.077	0.584 ± 0.063	4.111
		Pb–Pb positive	Central	0.205 ± 0.002	0.772 ± 0.001	0.001
		Negative	Central	0.205 ± 0.002	0.772 ± 0.001	0.001
		Positive	Peripheral	0.220 ± 0.017	0.697 ± 0.012	0.148
		Negative	Peripheral	0.220 ± 0.017	0.697 ± 0.012	0.148

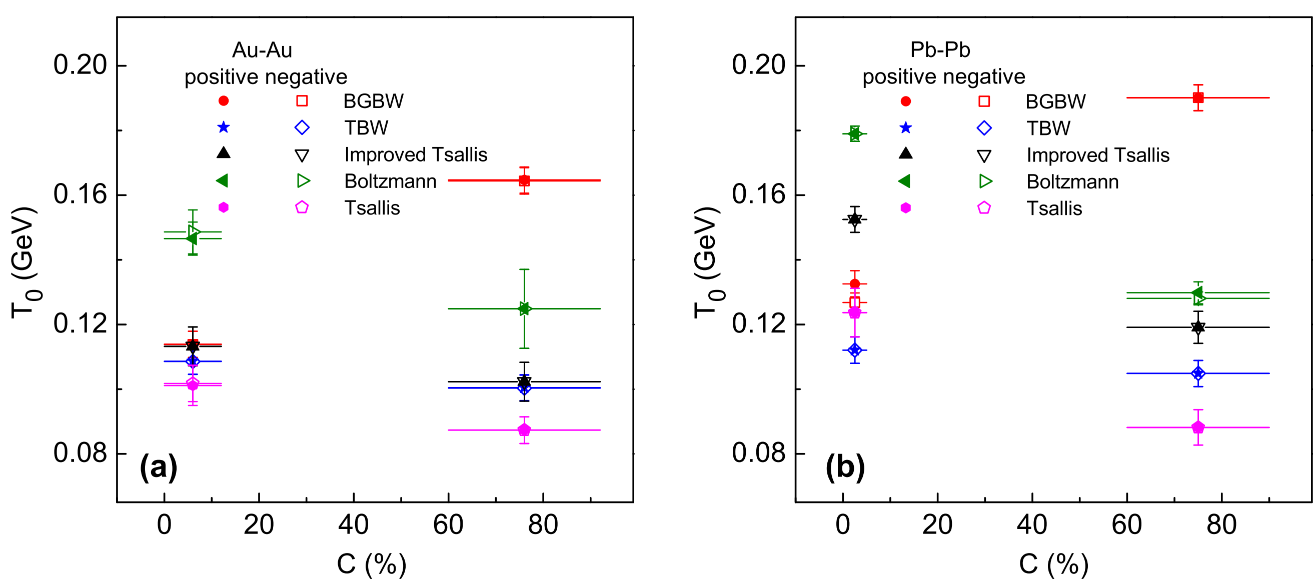

Fig. 6 (Color online) Comparisons of T_0 obtained by different methods for different centralities (C), where the values of T_0 in the first three methods are obtained by weighing different particles. Panels (**a**) and (**b**) correspond to the results for central (0–5 and 0–12%) and peripheral (80–92 and 60–80%) Au–Au collisions at $\sqrt{s_{NN}} = 200$ GeV and central (0–5%) and peripheral (80–90 and 60–80%) Pb–Pb collisions at $\sqrt{s_{NN}} = 2.76$ TeV respectively

shown in Figs. 8 and 9 which correspond to 200 GeV Au–Au and 2.76 TeV Pb–Pb collisions respectively. The data points are the same as Figs. 1 and 2 [25–29]. The dotted, solid, dashed, and dotted-dashed curves correspond to the results of method (1) with $n_0 = 1$ and 2, and of method (2) with $n_0 = 1$ and 2, respectively, where the results of

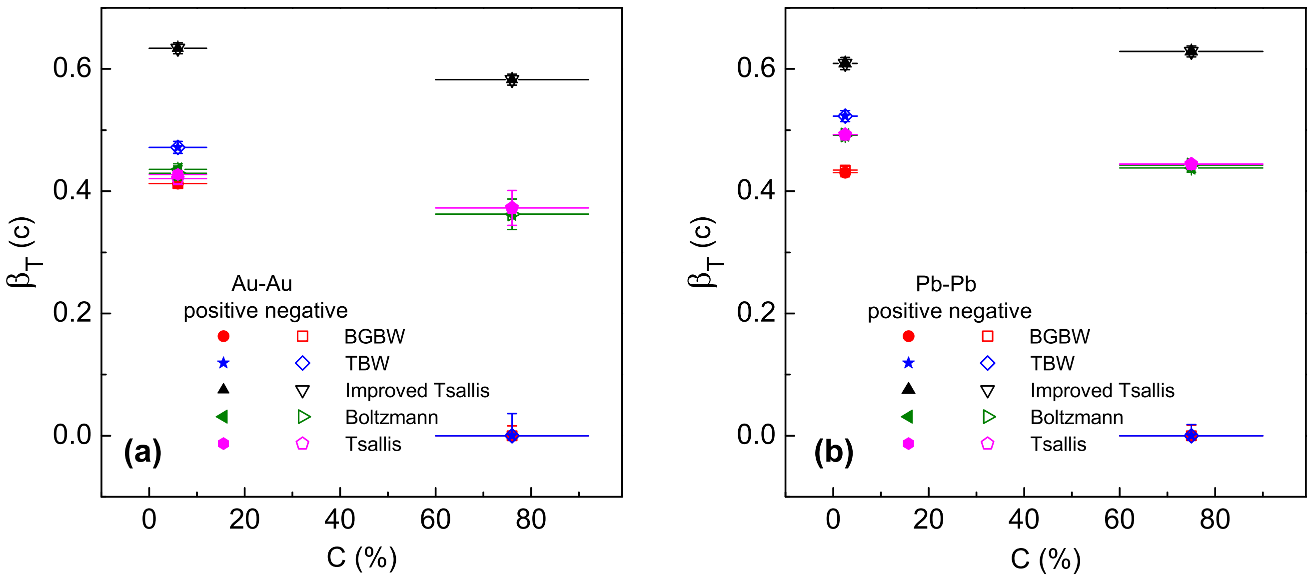

Fig. 7 (Color online) Same as Fig. 6, but showing the comparisons of β_T obtained by different methods for different centralities

method (1) with $n_0 = 2$ and of method (2) with $n_0 = 1$ in central collisions are the same as Figs. 1 and 2. The values of related parameters and χ^2/dof are listed in Tables 8 and 9, where the parameters for method (1) with $n_0 = 2$ and for method (2) with $n_0 = 1$ in central collisions repeat those in Tables 1 and 2, which are not listed again. One can see that, after the re-examination, the values of T_0 in central collisions are larger than those in peripheral collisions. The values of β_T in peripheral collisions are no longer zero. These new results are consistent with other methods.

To give new comparisons for T_0 and β_T, the new results obtained by the first two methods are shown in Figs. 10 and 11 respectively, where the results corresponding to method (1) for central collisions with $n_0 = 2$ and to method (2) for central collisions with $n_0 = 1$ are the same as those in Figs. 6 and 7. Combining Figs. 6, 7, 10 and 11, one can see that the four methods show approximately the consistent results. These comparisons enlighten us to use the first two methods in peripheral collisions by a non-zero β_T. After the re-examination for β_T in peripheral collisions, we obtain a relatively larger T_0 in central collisions for the four methods. In particular, the parameter T_0 at the LHC is slightly larger than or nearly equal to that at the RHIC, not only for central collisions but also for peripheral collisions. Except for method (3), the methods show a slightly larger or nearly invariant β_T in central collisions when compared with peripheral collisions, and when LHC comparing data from LHC with the RHIC, while method (3) shows nearly the same β_T in different centralities and at different energies.

We would like to point out that, in the re-examination for β_T in methods (1) and (2), we have assumed both β_T in central and peripheral collisions to be non-zero. In most cases [11, 14], both the conventional BGBW and TBW models used non-zero β_T in central collisions and zero (or almost zero) β_T in peripheral collisions. In the case of using a non-zero or zero (or almost zero) β_T in peripheral collisions, we can obtain a relatively smaller or larger T_0 compared with central collisions. Indeed, the selection of β_T in peripheral collisions is an important issue in both the BGBW and TBW models. In fact, β_T is a sensitive quantity which can affect T_0. The larger β_T that is selected, the smaller T_0 that is needed. The main correlation is between β_T and T_0, and the effect of n_0 is very small. In Figs. 1 and 2, we have used a zero β_T for peripheral collisions and obtained a harmonious result on the relative size of T_0 with Ref. [28] in which β_T ($0.35c$) for peripheral collisions is nearly a half of that ($0.65c$) for central collisions, and n_0 is also different from ours. While in Figs. 8 and 9, we have used a non-zero and slightly smaller β_T for peripheral collisions and obtained a different result from Ref. [28].

In order to make the conclusion more convincing, we can only fit the low p_T region of the particle spectra using the four methods with the same p_T cut to decrease the number of free fitting parameters. When the p_T cut increases from 2 to 3.5 GeV/c, T_0 (or T) increases or both T_0 (or T) and β_T increase slightly. The relative size of T_0 (β_T) obtained above for central and peripheral collisions is unchanged. In particular, β_T is also a sensitive quantity. For peripheral collisions, a zero or non-zero β_T in the first two methods can give different results. In our opinion, in central and peripheral collisions, it depends on β_T if we want to determine which T_0 is larger. We are inclined to use a non-zero β_T for peripheral collisions due to the small system which is similar to peripheral collisions in number of participant nucleons also showing collective expansion [40].

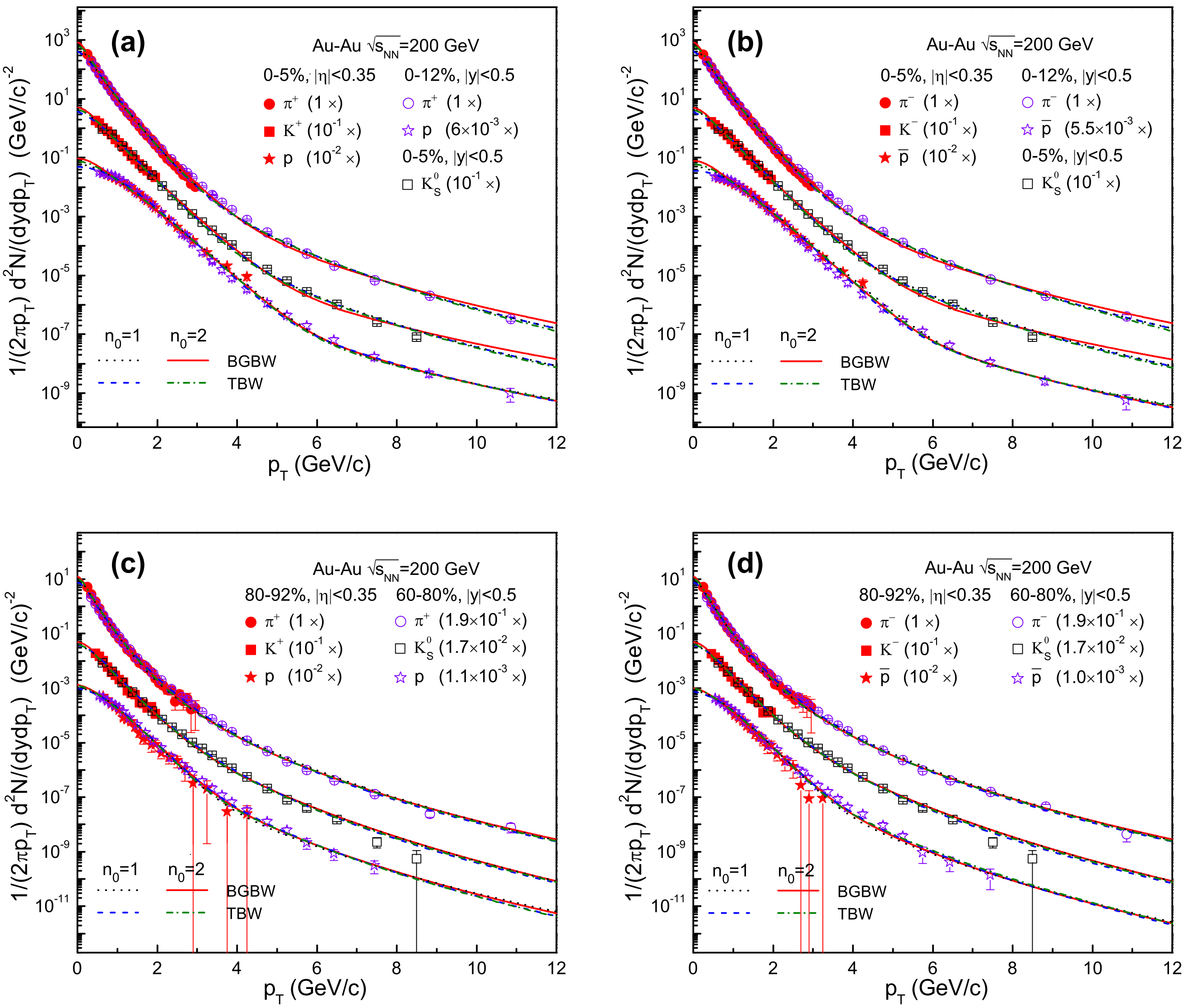

Fig. 8 (Color online) Reanalyzing the transverse momentum spectra [25–27] collected in Fig. 1 by the first two methods. The dotted, solid, dashed, and dotted-dashed curves are our results calculated by using method (1) with $n_0 = 1$ and 2, as well as method (2) with $n_0 = 1$ and 2, respectively. The results for central collisions obtained by method (1) with $n_0 = 2$ and by method (2) with $n_0 = 1$ are the same as Fig. 1

Compared with peripheral collisions, the larger T_0 in central collisions renders more deposition of collision energy and higher excitation of the interacting system due to more participating nucleons taking part in the violent collisions. Compared with the top RHIC energy, the larger T_0 at the LHC energy also renders more deposition of collision energy and higher excitation of interacting system due to higher $\sqrt{s_{NN}}$ at the LHC. At the same time, from the top RHIC to the LHC energies, a nearly invariant T_0 reflects the limiting deposition of collision energy. Compared with peripheral collisions, the slightly larger or nearly the same β_T in central collisions renders similar expansion in both the centralities. At the same time, at the top RHIC and LHC energies, the two systems also show similar expansion due to similar β_T.

It should be noted that, although Eq. (2) [14] does not implement the azimuthal integral over the freeze-out surface which gives rise to the modified Bessel functions in Eq. (1), it does not affect the extractions of kinetic freeze-out parameters due to the application of numerical integral. Although Eq. (3) [15, 16] assumes a single, infinitesimally thin shell of fixed flow velocity and also does not perform the integral over the freeze-out surface, it can extract the mean trend of kinetic freeze-out parameters. As for the alternative method [12, 17–20, 22–24], it assumes non-relativistic flow velocities in the expressions used to extract the freeze-out parameters, which is the case that β_T is indeed not too large at the top RHIC and LHC energies.

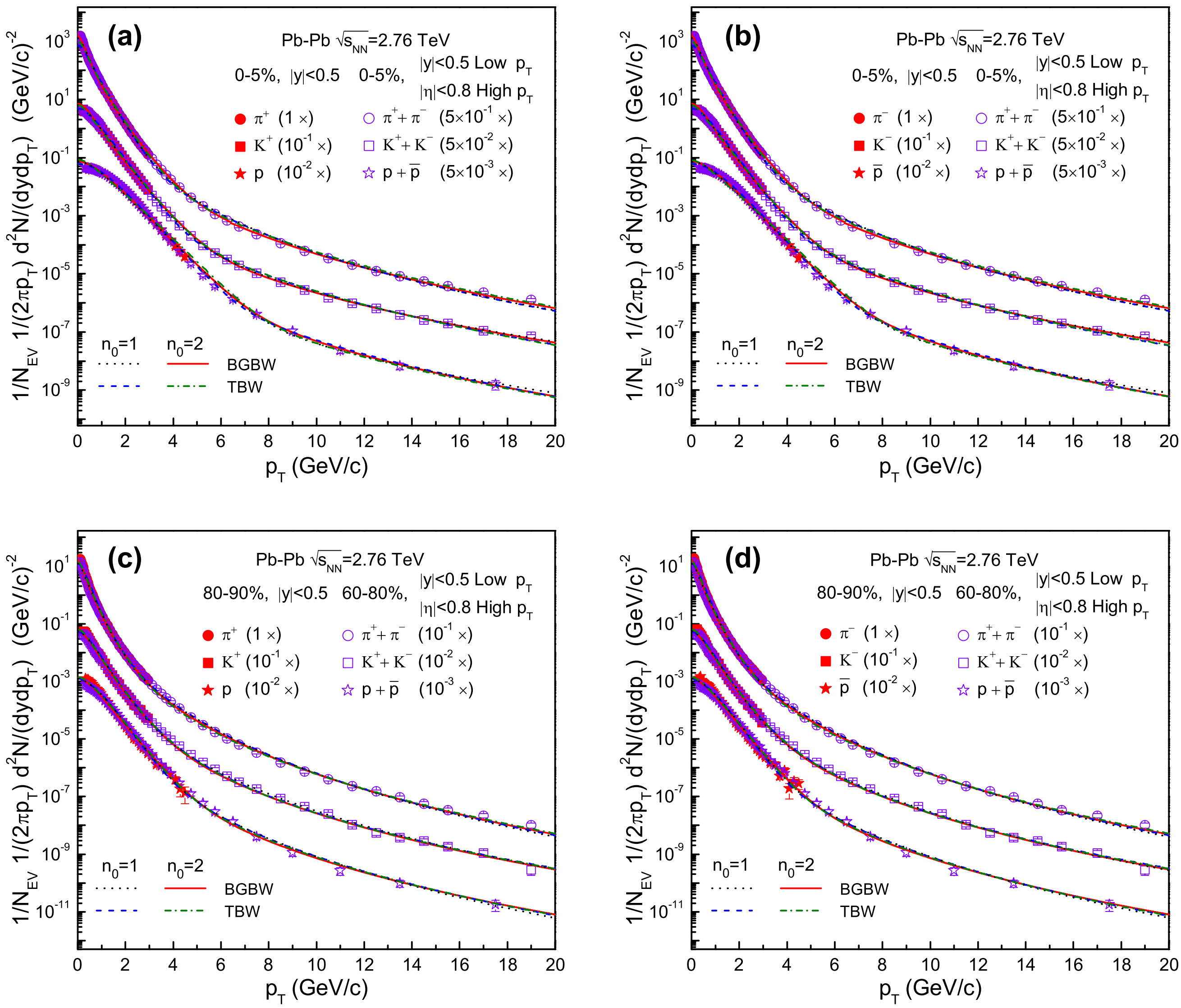

Fig. 9 (Color online) Same as Fig. 8, but reanalyzing the transverse momentum spectra [28, 29] collected in Fig. 2 by the first two methods. The results for central collisions obtained by method (1) with $n_0 = 2$ and by method (2) with $n_0 = 1$ are the same as Fig. 2

4 Conclusion

We summarize here our main observations and conclusions.

(a) The p_T spectra of $\pi^{\pm}$, $K^{\pm}$, K^0_S, p, and $\bar{p}$ produced in central (0–5 and 0–12%) and peripheral (80–92 and 60–80%) Au–Au collisions at $\sqrt{s_{NN}} = 200$ GeV and in central (0–5%) and peripheral (80–90 and 60–80%) Pb–Pb collisions at $\sqrt{s_{NN}} = 2.76$ TeV have been analyzed by a few different superpositions in which the distributions related to the extractions of T_0 and β_T are used for the soft component and the inverse power-law is used for the hard component. We have used five distributions for the soft component, (1) the Blast-Wave model with Boltzmann–Gibbs statistics, (2) the Blast-Wave model with Tsallis statistics, (3) the Tsallis distribution with flow effect, $(4)_a$ the Boltzmann distribution, and $(4)_b$ the Tsallis distribution. The first three distributions are in fact three methods for the extractions of T_0 and β_T. The last two distributions are used in the fourth method, i.e. the alternative method.

(b) The experimental data measured by the PHENIX, STAR, and ALICE Collaborations are fitted by the model results. Our calculations show that the parameter T_0 obtained by method (1) with the conventional treatment for central collisions is smaller than that for peripheral collisions, which is inconsistent with the results obtained by other model methods. In the conventional treatment, the parameter β_T in peripheral collisions is taken to be nearly

Table 8 Values of free parameters (T_0, β_T, k, p_0, and n), the normalization constant (N_0), and χ^2/dof corresponding to the fits of method (1) in Figs. 8 and 9, where the values for central collisions with $n_0 = 2$ in the self-similar flow profile repeat those in Table 1, which are not listed again

Figures	Cent.	Main Part.	T_0 (GeV)	β_T (c)	k	p_0 (GeV/c)	n	N_0	χ^2/dof
8(a)	Central	π^+	0.138 ± 0.005	0.452 ± 0.008	0.964 ± 0.006	2.375 ± 0.069	10.365 ± 0.188	633.869 ± 62.976	3.369
Au–Au		K^+	0.169 ± 0.005	0.412 ± 0.008	0.901 ± 0.006	1.998 ± 0.058	9.675 ± 0.185	54.966 ± 3.838	5.502
$n_0 = 1$		p	0.198 ± 0.005	0.398 ± 0.008	0.995 ± 0.002	2.485 ± 0.072	8.075 ± 0.171	8.457 ± 0.646	5.274
8(b)	Central	π^-	0.138 ± 0.005	0.452 ± 0.008	0.964 ± 0.006	2.375 ± 0.069	10.365 ± 0.188	633.869 ± 62.976	3.277
		K^-	0.169 ± 0.005	0.412 ± 0.008	0.901 ± 0.006	2.098 ± 0.060	9.835 ± 0.188	54.759 ± 3.823	6.405
		$\bar{p}$	0.198 ± 0.005	0.397 ± 0.008	0.994 ± 0.002	2.185 ± 0.070	7.975 ± 0.168	7.096 ± 0.649	12.058
8(c)	Peripheral	π^+	0.115 ± 0.005	0.415 ± 0.008	0.901 ± 0.008	2.512 ± 0.079	11.123 ± 0.173	11.713 ± 0.591	4.455
		K^+	0.145 ± 0.005	0.415 ± 0.008	0.888 ± 0.008	3.923 ± 0.082	12.923 ± 0.178	0.482 ± 0.077	6.711
		p	0.157 ± 0.006	0.353 ± 0.008	0.947 ± 0.008	3.316 ± 0.069	11.016 ± 0.169	0.142 ± 0.015	1.444
8(d)	Peripheral	π^-	0.115 ± 0.005	0.415 ± 0.008	0.901 ± 0.008	2.512 ± 0.079	11.123 ± 0.173	11.713 ± 0.591	3.800
		K^-	0.145 ± 0.005	0.415 ± 0.008	0.888 ± 0.008	3.923 ± 0.082	12.923 ± 0.178	0.482 ± 0.077	5.907
		$\bar{p}$	0.157 ± 0.006	0.353 ± 0.008	0.945 ± 0.008	3.316 ± 0.069	11.528 ± 0.169	0.112 ± 0.011	0.904
8(c)	Peripheral	π^+	0.103 ± 0.005	0.395 ± 0.008	0.896 ± 0.008	2.012 ± 0.063	10.203 ± 0.185	14.240 ± 1.308	2.956
Au–Au		K^+	0.117 ± 0.006	0.383 ± 0.008	0.901 ± 0.008	3.983 ± 0.071	12.993 ± 0.195	0.636 ± 0.033	4.221
$n_0 = 2$		p	0.118 ± 0.006	0.355 ± 0.008	0.905 ± 0.008	3.268 ± 0.066	11.506 ± 0.186	0.170 ± 0.012	1.093
8(d)	Peripheral	π^-	0.103 ± 0.005	0.395 ± 0.008	0.896 ± 0.008	2.012 ± 0.063	10.203 ± 0.185	14.240 ± 1.308	2.652
		K^-	0.117 ± 0.006	0.383 ± 0.008	0.901 ± 0.008	3.983 ± 0.071	12.993 ± 0.195	0.636 ± 0.033	3.879
		$\bar{p}$	0.118 ± 0.006	0.355 ± 0.008	0.905 ± 0.008	3.268 ± 0.066	11.926 ± 0.186	0.128 ± 0.012	0.589
9(a)	Central	π^+	0.149 ± 0.005	0.473 ± 0.008	0.922 ± 0.008	1.535 ± 0.056	7.276 ± 0.104	1465.409 ± 127.197	3.815
Pb–Pb		K^+	0.235 ± 0.005	0.399 ± 0.008	0.938 ± 0.008	1.295 ± 0.055	6.114 ± 0.101	77.086 ± 7.666	1.463
$n_0 = 1$		p	0.338 ± 0.005	0.332 ± 0.006	0.991 ± 0.002	2.285 ± 0.082	6.485 ± 0.108	10.152 ± 0.330	11.411
9(b)	Central	π^-	0.149 ± 0.005	0.473 ± 0.008	0.922 ± 0.008	1.535 ± 0.056	7.276 ± 0.104	1465.409 ± 127.197	3.751
		K^-	0.235 ± 0.005	0.399 ± 0.008	0.938 ± 0.008	1.295 ± 0.055	6.114 ± 0.101	77.157 ± 7.674	1.229
		$\bar{p}$	0.338 ± 0.005	0.332 ± 0.006	0.991 ± 0.002	2.285 ± 0.082	6.485 ± 0.108	10.152 ± 0.330	10.234
9(c)	Peripheral	π^+	0.127 ± 0.005	0.473 ± 0.008	0.934 ± 0.008	2.793 ± 0.078	8.765 ± 0.138	14.233 ± 0.756	8.290
		K^+	0.169 ± 0.004	0.453 ± 0.008	0.902 ± 0.008	2.665 ± 0.074	7.995 ± 0.129	0.723 ± 0.050	2.448
		p	0.180 ± 0.005	0.436 ± 0.008	0.918 ± 0.008	2.995 ± 0.092	8.599 ± 0.132	0.167 ± 0.014	3.944
9(d)	Peripheral	π^-	0.127 ± 0.005	0.473 ± 0.008	0.934 ± 0.008	2.793 ± 0.078	8.765 ± 0.138	14.233 ± 0.756	8.285
		K^-	0.169 ± 0.004	0.453 ± 0.008	0.902 ± 0.008	2.665 ± 0.074	7.995 ± 0.129	0.723 ± 0.050	2.686
		$\bar{p}$	0.180 ± 0.005	0.436 ± 0.008	0.918 ± 0.008	2.995 ± 0.092	8.599 ± 0.132	0.167 ± 0.014	4.196
9(c)	Peripheral	π^+	0.116 ± 0.004	0.410 ± 0.008	0.941 ± 0.007	2.393 ± 0.058	8.185 ± 0.153	17.976 ± 0.731	4.533
Pb–Pb		K^+	0.184 ± 0.005	0.367 ± 0.008	0.908 ± 0.007	2.375 ± 0.056	7.585 ± 0.145	0.702 ± 0.044	1.120
$n_0 = 2$		p	0.204 ± 0.005	0.343 ± 0.008	0.919 ± 0.007	2.178 ± 0.055	7.515 ± 0.145	0.172 ± 0.015	1.791
9(d)	Peripheral	π^-	0.116 ± 0.004	0.410 ± 0.008	0.941 ± 0.007	2.393 ± 0.058	8.185 ± 0.153	17.976 ± 0.731	4.601
		K^-	0.184 ± 0.005	0.367 ± 0.008	0.908 ± 0.007	2.375 ± 0.056	7.585 ± 0.145	0.702 ± 0.044	1.232
		$\bar{p}$	0.204 ± 0.005	0.343 ± 0.008	0.919 ± 0.007	2.178 ± 0.055	7.515 ± 0.145	0.172 ± 0.015	1.963

Table 9 Values of free parameters (T_0, q, β_T, k, p_0, and n), the normalization constant (N_0), and χ^2/dof corresponding to the fits of method (2) in Figs. 8 and 9, where the values for central collisions with $n_0 = 1$ in the self-similar flow profile repeat those in Table 2, which are not listed again

Figures	Cent.	Main Part.	T_0 (GeV)	q	β_T (c)	k	p_0 (GeV/c)	n	N_0	χ^2/dof
8(c)	Peripheral	π^+	0.079 ± 0.004	1.069 ± 0.006	0.405 ± 0.009	0.924 ± 0.006	2.192 ± 0.083	10.379 ± 0.189	9.197 ± 0.912	1.715
Au–Au		K^+	0.089 ± 0.005	1.063 ± 0.005	0.389 ± 0.009	0.921 ± 0.006	3.602 ± 0.096	12.282 ± 0.165	0.491 ± 0.052	4.499
$n_0 = 1$		p	0.095 ± 0.005	1.028 ± 0.005	0.389 ± 0.009	0.902 ± 0.007	3.810 ± 0.102	12.568 ± 0.171	0.134 ± 0.010	1.457
8(d)	Peripheral	π^-	0.079 ± 0.004	1.069 ± 0.006	0.405 ± 0.009	0.924 ± 0.006	2.192 ± 0.083	10.379 ± 0.189	9.197 ± 0.912	1.445
		K^-	0.089 ± 0.005	1.061 ± 0.005	0.389 ± 0.009	0.921 ± 0.006	3.602 ± 0.096	12.282 ± 0.165	0.486 ± 0.052	3.127
		$\bar{p}$	0.095 ± 0.005	1.028 ± 0.005	0.389 ± 0.009	0.908 ± 0.007	3.810 ± 0.102	12.868 ± 0.171	0.100 ± 0.010	0.670
8(a)	Central	π^+	0.091 ± 0.003	1.010 ± 0.005	0.401 ± 0.008	0.985 ± 0.003	3.591 ± 0.091	12.035 ± 0.173	683.617 ± 48.090	3.630
Au–Au		K^+	0.103 ± 0.005	1.008 ± 0.004	0.395 ± 0.007	0.961 ± 0.004	2.675 ± 0.103	10.327 ± 0.089	51.119 ± 5.034	5.703
$n_0 = 2$		p	0.118 ± 0.005	1.009 ± 0.004	0.374 ± 0.005	0.997 ± 0.002	3.385 ± 0.168	8.895 ± 0.108	9.706 ± 0.421	6.866
8(b)	Central	π^-	0.091 ± 0.003	1.010 ± 0.005	0.401 ± 0.008	0.985 ± 0.003	3.591 ± 0.091	12.035 ± 0.173	683.617 ± 48.090	3.362
		K^-	0.103 ± 0.005	1.008 ± 0.004	0.395 ± 0.007	0.961 ± 0.004	2.675 ± 0.103	10.327 ± 0.159	49.059 ± 5.034	6.731
		$\bar{p}$	0.118 ± 0.005	1.009 ± 0.004	0.374 ± 0.005	0.997 ± 0.002	3.385 ± 0.168	9.095 ± 0.112	7.862 ± 0.422	15.669
8(c)	Peripheral	π^+	0.073 ± 0.004	1.025 ± 0.004	0.398 ± 0.008	0.943 ± 0.004	2.653 ± 0.091	11.093 ± 0.169	10.627 ± 0.888	3.602
		K^+	0.082 ± 0.005	1.033 ± 0.005	0.380 ± 0.008	0.891 ± 0.005	3.683 ± 0.092	12.553 ± 0.170	0.470 ± 0.005	4.498
		p	0.085 ± 0.005	1.009 ± 0.005	0.359 ± 0.008	0.910 ± 0.005	3.950 ± 0.093	12.756 ± 0.181	0.150 ± 0.013	1.306
8(d)	Peripheral	π^-	0.073 ± 0.004	1.025 ± 0.004	0.398 ± 0.008	0.943 ± 0.004	2.653 ± 0.091	11.093 ± 0.169	10.627 ± 0.888	3.239
		K^-	0.082 ± 0.005	1.033 ± 0.005	0.380 ± 0.008	0.891 ± 0.005	3.683 ± 0.092	12.553 ± 0.170	0.470 ± 0.052	3.570
		$\bar{p}$	0.085 ± 0.005	1.009 ± 0.005	0.359 ± 0.008	0.910 ± 0.005	3.950 ± 0.093	13.018 ± 0.181	0.117 ± 0.011	0.647
9(c)	Peripheral	π^+	0.089 ± 0.004	1.041 ± 0.005	0.446 ± 0.010	0.929 ± 0.006	2.403 ± 0.075	8.398 ± 0.169	14.318 ± 0.567	12.971
Pb–Pb		K^+	0.099 ± 0.005	1.065 ± 0.005	0.446 ± 0.010	0.926 ± 0.006	2.375 ± 0.071	7.468 ± 0.153	0.650 ± 0.062	1.544
$n_0 = 1$		p	0.110 ± 0.005	1.030 ± 0.005	0.446 ± 0.010	0.894 ± 0.007	2.415 ± 0.077	8.005 ± 0.161	0.157 ± 0.014	2.881
9(d)	Peripheral	π^-	0.089 ± 0.004	1.041 ± 0.005	0.446 ± 0.010	0.929 ± 0.006	2.403 ± 0.075	8.398 ± 0.169	14.318 ± 0.567	12.947
		K^-	0.099 ± 0.005	1.065 ± 0.005	0.446 ± 0.010	0.926 ± 0.006	2.375 ± 0.071	7.468 ± 0.153	0.650 ± 0.062	1.724
		$\bar{p}$	0.110 ± 0.005	1.030 ± 0.005	0.446 ± 0.010	0.894 ± 0.007	2.415 ± 0.077	8.005 ± 0.161	0.157 ± 0.014	3.065
9(a)	Central	π^+	0.099 ± 0.005	1.006 ± 0.004	0.435 ± 0.006	0.989 ± 0.003	2.775 ± 0.085	7.515 ± 0.158	1099.140 ± 107.121	2.897
Pb–Pb		K^+	0.113 ± 0.005	1.002 ± 0.001	0.435 ± 0.006	0.984 ± 0.003	3.575 ± 0.101	7.735 ± 0.115	73.563 ± 7.358	3.623
$n_0 = 2$		p	0.155 ± 0.005	1.002 ± 0.001	0.419 ± 0.004	0.996 ± 0.002	4.975 ± 0.109	8.225 ± 0.128	10.566 ± 0.284	15.778
9(b)	Central	π^-	0.099 ± 0.005	1.006 ± 0.004	0.435 ± 0.006	0.989 ± 0.003	2.775 ± 0.085	7.515 ± 0.158	1099.140 ± 107.121	2.955
		K^-	0.113 ± 0.005	1.002 ± 0.001	0.435 ± 0.006	0.984 ± 0.003	3.575 ± 0.101	7.735 ± 0.115	73.563 ± 7.358	3.282
		$\bar{p}$	0.155 ± 0.005	1.002 ± 0.001	0.419 ± 0.004	0.996 ± 0.002	4.975 ± 0.109	8.225 ± 0.128	9.983 ± 0.278	14.519
9(c)	Peripheral	π^+	0.079 ± 0.004	1.045 ± 0.005	0.405 ± 0.008	0.976 ± 0.004	3.003 ± 0.095	8.335 ± 0.129	14.692 ± 0.760	7.361
		K^+	0.086 ± 0.005	1.053 ± 0.005	0.399 ± 0.008	0.928 ± 0.004	2.375 ± 0.089	7.475 ± 0.121	0.760 ± 0.084	0.975
		p	0.102 ± 0.005	1.025 ± 0.005	0.385 ± 0.007	0.940 ± 0.006	2.675 ± 0.092	7.965 ± 0.126	0.177 ± 0.014	2.380
9(d)	Peripheral	π^-	0.079 ± 0.004	1.045 ± 0.005	0.405 ± 0.008	0.976 ± 0.004	3.003 ± 0.095	8.335 ± 0.129	14.692 ± 0.760	7.488
		K^-	0.086 ± 0.005	1.053 ± 0.005	0.399 ± 0.008	0.928 ± 0.004	2.375 ± 0.089	7.475 ± 0.121	0.760 ± 0.084	1.069
		$\bar{p}$	0.102 ± 0.005	1.025 ± 0.005	0.385 ± 0.007	0.940 ± 0.006	2.675 ± 0.092	7.965 ± 0.126	0.171 ± 0.014	2.410

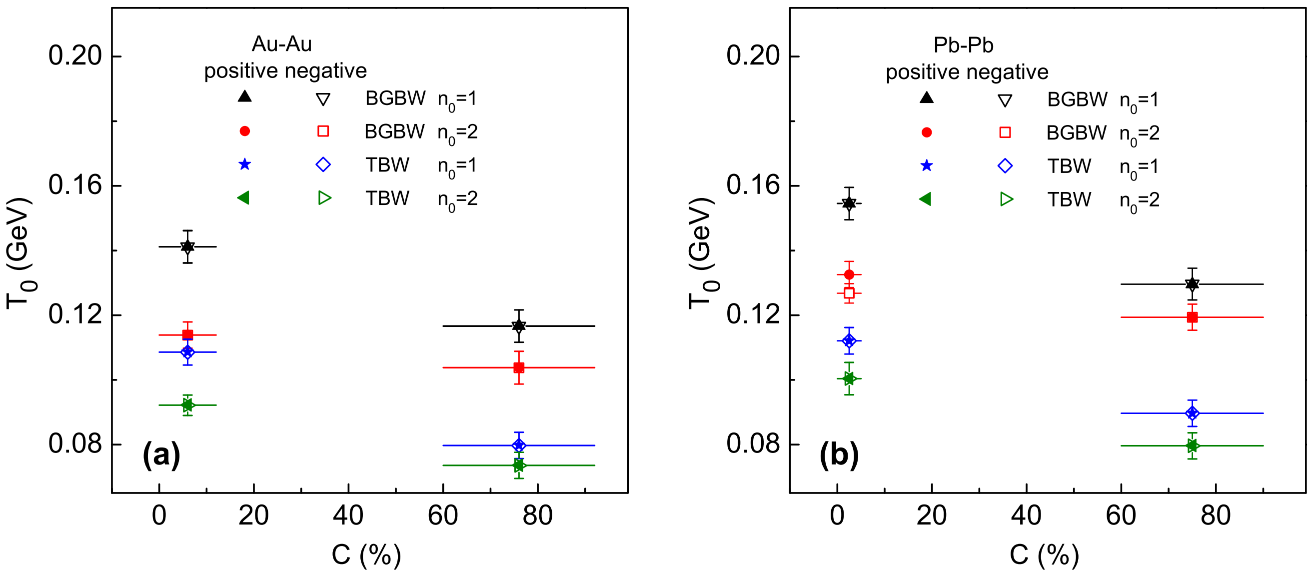

Fig. 10 (Color online) Comparisons of T_0 obtained by the first two methods with $n_0 = 1$ and 2 for different centralities. **a** and **b** correspond to the results for central (0–5 and 0–12%) and peripheral (80–92 and 60–80%) Au–Au collisions at $\sqrt{s_{NN}} = 200$ GeV and central (0–5%) and peripheral (80–90 and 60–80%) Pb–Pb collisions at $\sqrt{s_{NN}} = 2.76$ TeV, respectively. The values of T_0 are obtained by weighing different particles and the results for central collisions obtained by method (1) with $n_0 = 2$ and by method (2) with $n_0 = 1$ are the same as Fig. 6

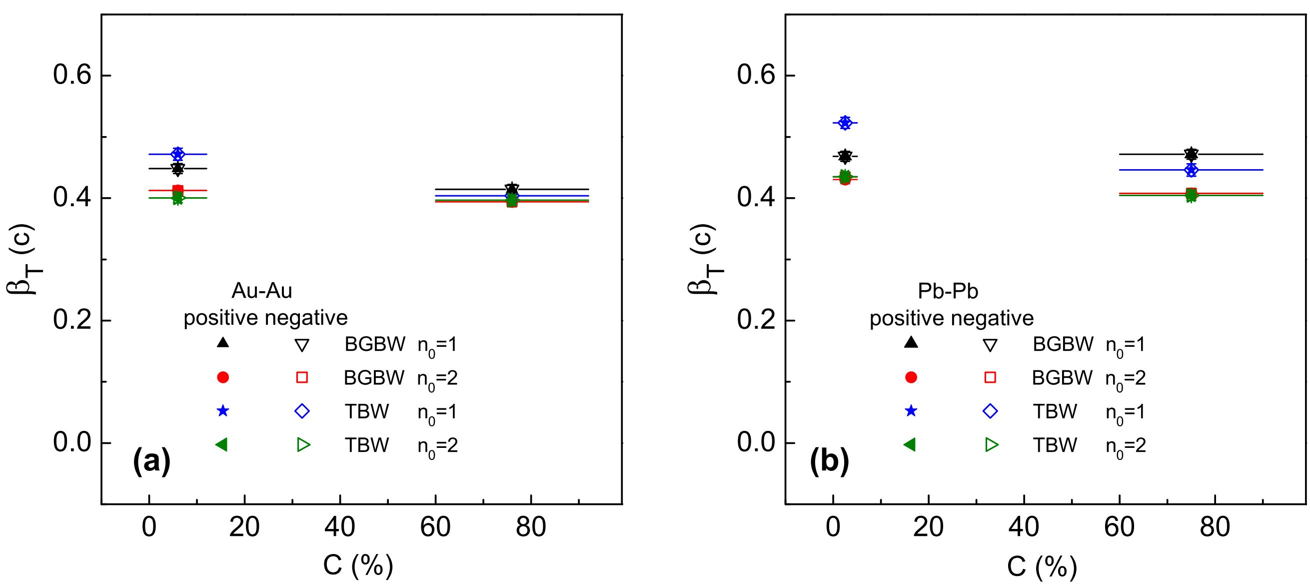

Fig. 11 (Color online) Same as Fig. 10, but showing the comparisons of β_T obtained by the first two methods for different centralities. The results for central collisions obtained by method (1) with $n_0 = 2$ and by method (2) with $n_0 = 1$ are the same as Fig. 7

zero, which results in a larger T_0 than normal. By using the conventional treatment, both methods (1) and (2) show a nearly zero β_T value in the peripheral collisions according to Refs. [11, 14], while other methods show a considerable β_T in both central and peripheral collisions.

(c) In central and peripheral collisions, we have to select a suitable β_T so that we can determine which T_0 is larger. We are inclined to use a non-zero β_T for peripheral collisions due to the small system also showing collective expansion. We have given a re-examination for β_T in peripheral collisions in methods (1) and (2) in which β_T is taken to be $\sim (0.40 \pm 0.07)c$. By using a non-zero β_T, the first two methods show approximately consistent results with other methods, not only for T_0 but also for β_T, though method (3) gives a larger β_T. We have uniformly obtained a larger T_0 in central collisions by the four methods. In particular, the parameter T_0 at the LHC is larger than or equal to that at the RHIC. Except for method (3), the methods show a slightly larger or nearly invariant β_T in central collisions compared to peripheral collisions, and at the LHC compared with the RHIC.

(d) The new results obtained by the widely used Blast-Wave model with Boltzmann–Gibbs or Tsallis statistics are in agreement with those obtained by the newly used alternative method which uses the Boltzmann or Tsallis distribution. This consistency confirms the validity of the alternative method. The result that the central collisions have a larger T_0 renders more deposition of collision energy and higher excitation of the interacting system due to more participating nucleons taking part in the violent collisions. From the RHIC to LHC, the slightly increased or nearly invariant T_0 renders the limiting or maximum deposition of collisions energy. From central to peripheral collisions and from the RHIC to LHC, the slightly increased or nearly invariant β_T renders the limiting or maximum blast of the interacting system.

References

1. N. Xu, (for the STAR Collaboration), An overview of STAR experimental results. Nucl. Phys. A **931**, 1 (2014). https://doi.org/10.1016/j.nuclphysa.2014.10.022
2. S. Chatterjee, S. Das, L. Kumar et al., Freeze-out parameters in heavy-ion collisions at AGS, SPS, RHIC, and LHC energies. Adv. High Energy Phys. **2015**, 349013 (2015). https://doi.org/10.1155/2015/349013
3. S. Chatterjee, B. Mohanty, R. Singh, Freezeout hypersurface at energies available at the CERN Large Hadron Collider from particle spectra: Flavor and centrality dependence. Phys. Rev. C **92**, 024917 (2015). https://doi.org/10.1103/PhysRevC.92.024917
4. S. Chatterjee, B. Mohanty, Production of light nuclei in heavy-ion collisions within a multiple-freezeout scenario. Phys. Rev. C **90**, 034908 (2014). https://doi.org/10.1103/PhysRevC.90.034908
5. S.S. Räsänen, (for the ALICE Collaboration). ALICE overview. EPJ Web Conf. **126**, 02026 (2016) https://doi.org/10.1051/epjconf/201612602026
6. M. Floris, Hadron yields and the phase diagram of strongly interacting matter. Nucl. Phys. A **931**, 103 (2014). https://doi.org/10.1016/j.nuclphysa.2014.09.002
7. S. Das, D. Mishra, S. Chatterjee et al., Freeze-out conditions in proton-proton collisions at the highest energies available at the BNL Relativistic Heavy Ion Collider and the CERN Large Hadron Collider. Phys. Rev. C **95**, 014912 (2017). https://doi.org/10.1103/PhysRevC.95.014912
8. P. Huovinen, Chemical freeze-out temperature in the hydrodynamical description of Au+Au collisions at $\sqrt{s_{NN}} = 200$ GeV. Eur. Phys. J. A **37**, 121 (2008). https://doi.org/10.1140/epja/i2007-10611-3
9. B. De, Non-extensive statistics and understanding particle production and kinetic freeze-out process from p_T-spectra at 2.76 TeV. Eur. Phys. J. A **50**, 138 (2014). https://doi.org/10.1140/epja/i2014-14138-2
10. A. Andronic, An overview of the experimental study of quark-gluon matter in high-energy nucleus-nucleus collisions. Int. J. Mod. Phys. A **29**, 1430047 (2014). https://doi.org/10.1142/S0217751X14300476
11. E. Schnedermann, J. Sollfrank, U. Heinz, Thermal phenomenology of hadrons from 200*A* GeV S+S collisions. Phys. Rev. C **48**, 2462 (1993). https://doi.org/10.1103/PhysRevC.48.2462
12. B.I. Abelev et al., (STAR Collaboration), Systematic measurements of identified particle spectra in pp, d+Au, and Au+Au collisions at the STAR detector. Phys. Rev. C **79**, 034909 (2009). https://doi.org/10.1103/PhysRevC.79.034909
13. B.I. Abelev et al., (STAR Collaboration), Identified particle production, azimuthal anisotropy, and interferometry measurements in Au+Au collisions at $\sqrt{s_{NN}} = 9.2$ GeV. Phys. Rev. C **81**, 024911 (2010). https://doi.org/10.1103/PhysRevC.81.024911
14. Z.B. Tang, Y.C. Xu, L.J. Ruan et al., Spectra and radial flow in relativistic heavy ion collisions with Tsallis statistics in a blast-wave description. Phys. Rev. C **79**, 051901(R) (2009). https://doi.org/10.1103/PhysRevC.79.051901
15. T. Bhattacharyya, J. Cleymans, A. Khuntia et al., Radial flow in non-extensive thermodynamics and study of particle spectra at LHC in the limit of small $(q-1)$. Eur. Phys. J. A **52**, 30 (2016). https://doi.org/10.1140/epja/i2016-16030-5
16. D. Thakur, S. Tripathy, P. Garg et al., Indication of a differential freeze-out in proton-proton and heavy-ion collisions at RHIC and LHC energies. Adv. High Energy Phys. **2016**, 4149352 (2016). https://doi.org/10.1155/2016/4149352
17. S. Takeuchi, K. Murase, T. Hirano, P. Huovinen, Y. Nara, Effects of hadronic rescattering on multistrange hadrons in high-energy nuclear collisions. Phys. Rev. C **92**, 044907 (2015). https://doi.org/10.1103/PhysRevC.92.044907
18. H. Heiselberg, A.-M. Levy, Elliptic flow and Hanbury–Brown–Twiss correlations in noncentral nuclear collisions. Phys. Rev. C **59**, 2716 (1999). https://doi.org/10.1103/PhysRevC.59.2716
19. U.W. Heinz, Lecture Notes for lectures presented at the 2nd CERN–Latin-American School of High-Energy Physics, June 1–14, 2003, San Miguel Regla, Mexico (2004), arXiv:hep-ph/0407360
20. R. Russo, Measurement of D^+ meson production in p-Pb collisions with the ALICE detector, Ph.D. Thesis, Universita degli Studi di Torino, Italy (2015), arXiv:1511.04380 [nucl-ex]
21. F.-H. Liu, Y.-Q. Gao, H.-R. Wei, On descriptions of particle transverse momentum spectra in high energy collisions. Adv. High Energy Phys. **2014**, 293873 (2014). https://doi.org/10.1155/2014/293873
22. H.-R. Wei, F.-H. Liu, R.A. Lacey, Kinetic freeze-out temperature and flow velocity extracted from transverse momentum spectra of final-state light flavor particles produced in collisions at RHIC and LHC. Eur. Phys. J. A **52**, 102 (2016). https://doi.org/10.1140/epja/i2016-16102-6
23. H.-L. Lao, H.-R. Wei, F.-H. Liu et al., An evidence of mass-dependent differential kinetic freeze-out scenario observed in Pb-Pb collisions at 2.76 TeV. Eur. Phys. J. A **52**, 203 (2016). https://doi.org/10.1140/epja/i2016-16203-2
24. H.-R. Wei, F.-H. Liu, R.A. Lacey, Disentangling random thermal motion of particles and collective expansion of source from transverse momentum spectra in high energy collisions. J. Phys. G **43**, 125102 (2016). https://doi.org/10.1088/0954-3899/43/12/125102
25. S.S. Adler et al., (PHENIX Collaboration), Identified charged particle spectra and yields in Au+Au collisions at $\sqrt{s_{NN}} = 200$

GeV. Phys. Rev. C **69**, 034909 (2004). https://doi.org/10.1103/PhysRevC.69.034909
26. B.I. Abelev et al., (STAR Collaboration), Identified baryon and meson distributions at large transverse momenta from Au+Au collisions at $\sqrt{s_{NN}} = 200$ GeV. Phys. Rev. Lett. **97**, 152301 (2006). https://doi.org/10.1103/PhysRevLett.97.152301
27. G. Agakishiev et al., (STAR Collaboration), Identified hadron compositions in $p+p$ and Au+Au collisions at high transverse momenta at $\sqrt{s_{NN}} = 200$ GeV. Phys. Rev. Lett. **108**, 072302 (2012). https://doi.org/10.1103/PhysRevLett.108.072302
28. B. Abelev et al., (ALICE Collaboration), Centrality dependence of π, K, and p in Pb-Pb collisions at $\sqrt{s_{NN}} = 2.76$ TeV. Phys. Rev. C **88**, 044910 (2013). https://doi.org/10.1103/PhysRevC.88.044910
29. J. Adam et al., (ALICE Collaboration), Centrality dependence of the nuclear modification factor of charged pions, kaons, and protons in Pb-Pb collisions at $\sqrt{s_{NN}} = 2.76$ TeV. Phys. Rev. C **93**, 034913 (2016). https://doi.org/10.1103/PhysRevC.93.034913
30. E. Schnedermann, U. Heinz, Relativistic hydrodynamics in a global fashion. Phys. Rev. C **47**, 1738 (1993). https://doi.org/10.1103/PhysRevC.47.1738
31. L. Kumar, (for the STAR Collaboration), Systematics of kinetic freeze-out properties in high energy collisions from STAR. Nucl. Phys. A **931**, 1114 (2014). https://doi.org/10.1016/j.nuclphysa.2014.08.085
32. H. Zheng, L.L. Zhu, Comparing the Tsallis distribution with and without thermodynamical description in $p+p$ collisions. Adv. High Energy Phys. **2016**, 9632126 (2016). https://doi.org/10.1155/2016/9632126
33. J. Cleymans, D. Worku, Relativistic thermodynamics: Transverse momentum distributions in high-energy physics. Eur. Phys. J. A **48**, 160 (2012). https://doi.org/10.1140/epja/i2012-12160-0
34. R. Odorico, Does a transverse energy trigger actually trigger on large-p_T jets? Phys. Lett. B **118**, 151 (1982). https://doi.org/10.1016/0370-2693(82)90620-7
35. G. Arnison et al., (UA1 Collaboration), Transverse momentum spectra for charged particles at the CERN proton-antiproton collider. Phys. Lett. B **118**, 167 (1982). https://doi.org/10.1016/0370-2693(82)90623-2
36. T. Mizoguchi, M. Biyajima, N. Suzuki, Analyses of whole transverse momentum distributions in $p\bar{p}$ and pp collisions by using a modified version of Hagedorn's formula. Int. J. Mod. Phys. A **32**, 1750057 (2017). https://doi.org/10.1142/S0217751X17500579
37. H.-L. Lao, F.-H. Liu, R.A. Lacey, Extracting kinetic freeze-out temperature and radial flow velocity from an improved Tsallis distribution. Eur. Phys. J. A 53, 44 (2017). https://doi.org/10.1140/epja/i2017-12238-1; and Erratum. Eur. Phys. J. A **53**, 143 (2017). https://doi.org/10.1140/epja/i2017-12333-3
38. F.-H. Liu, Y.-Q. Gao, B.-C. Li, Comparing two-Boltzmann distribution and Tsallis statistics of particle transverse momentums in collisions at LHC energies. Eur. Phys. J. A **50**, 123 (2014). https://doi.org/10.1140/epja/i2014-14123-9
39. H. Zheng, L.L. Zhu, Can Tsallis distribution fit all the particle spectra produced at RHIC and LHC? Adv. High Energy Phys. **2015**, 180491 (2015). https://doi.org/10.1155/2015/180491
40. H.C. Song, Y. Zhou, K. Gajdošová, Collective flow and hydrodynamics in large and small systems at the LHC. Nucl. Sci. Tech. **28**, 99 (2017). https://doi.org/10.1007/s41365-017-0245-4